Molecular Therapy
Original Article

Astrocyte-derived exosomal lncRNA 4933431K23Rik modulates microglial phenotype and improves post-traumatic recovery via SMAD7 regulation

Xuejun He,[1,2,8] Yimin Huang,[1,8] Yuan Liu,[1] Xincheng Zhang,[1] Quanji Wang,[1] Yanchao Liu,[1] Xiaopeng Ma,[1] Xiaobing Long,[3] Yang Ruan,[4] Hongxia Lei,[4] Chao Gan,[1] Xiaochuan Wang,[5] Xin Zou,[6] Bo Xiong,[7] Kai Shu,[1] Ting Lei,[1] and Huaqiu Zhang[1]

[1]Department of Neurosurgery, Tongji Hospital of Tongji Medical College of Huazhong University of Science and Technology, Jiefang Avenue 1095, Wuhan, Hubei 430030, P.R. China; [2]Department of Neurosurgery, First Affiliated Hospital, School of Medicine, Shihezi University, Shihezi, Xinjiang 832008, P.R. China; [3]Department of Emergency, Renmin Hospital of Wuhan University, Wuhan, Hubei 430060, P.R. China; [4]Wuhan United Imaging Life Science Instruments Ltd., Wuhan, Hubei 430030, P.R. China; [5]Department of Pathophysiology, School of Basic Medicine, Key Laboratory of Ministry of Education of China for Neurological Disorders, Tongji Medical College, Huazhong University of Science and Technology, Wuhan, Hubei 430030, P.R. China; [6]Institute of Integrated Traditional Chinese and Western Medicine, Tongji Hospital of Tongji Medical College of Huazhong University of Science and Technology, Wuhan, Hubei 430030, P.R. China; [7]Department of Forensic Medicine, Tongji Medical College, Huazhong University of Science and Technology, Wuhan, Hubei 430030, P.R. China

Astrocyte-microglial interaction plays a crucial role in brain injury-associated neuroinflammation. Our previous data illustrated that astrocytes secrete microRNA, leading to anti-inflammatory effects on microglia. Long non-coding RNAs participate in neuroinflammation regulation after traumatic brain injury. However, the effect of astrocytes on microglial phenotype via long non-coding RNAs and the underlying molecular mechanisms remain elusive. We used long non-coding RNA sequencing on murine astrocytes and found that exosomal long non-coding RNA 4933431K23Rik attenuated traumatic brain injury-induced microglial activation *in vitro* and *in vivo* and ameliorated cognitive function deficiency. Furthermore, microRNA and messenger RNA sequencing together with binding prediction illustrated that exosomal long non-coding RNA 4933431K23Rik up-regulates E2F7 and TFAP2C expression by sponging miR-10a-5p. Additionally, E2F7 and TFAP2C, as transcription factors, regulated microglial Smad7 expression. Using Cx3cr1-Smad7 overexpression of adeno-associated virus, microglia specifically overexpressed Smad7 in the attenuation of neuroinflammation, resulting in less cognitive deficiency after traumatic brain injury. Mechanically, overexpressed Smad7 physically binds to IκBα and inhibits its ubiquitination, preventing NF-κB signaling activation. The Smad7 activator asiaticoside alleviates neuroinflammation and protects neuronal function in traumatic brain injury mice. This study revealed that an exosomal long non-coding RNA from astrocytes attenuates microglial activation after traumatic brain injury by up-regulating Smad7, providing a potential therapeutic target.

INTRODUCTION

Traumatic brain injury (TBI) has a high incidence of death or functional disability, and is a major cause of mortality worldwide.[1] Apart from immediate neuronal damage which results in irreversible deficiencies, TBI-induced neuroinflammation is considered one of the major causes of secondary injury in the brain after TBI, which affects progression of recovery and prognosis.[1,2]

Glial cells comprise astrocytes, oligodendrocytes and microglia. As major supporting cells in the CNS, glial cells have a crucial role in the maintenance of brain homeostasis.[3,4] Microglia, the predominant immune cell type in the CNS, exhibit different phenotypes according to various stimuli which are classified as pro-inflammatory or anti-inflammatory.[5,6] Microglia were found to be one of the most important contributors to post-TBI neuroinflammation, which can affect patient prognosis.[1,7] Our previous study and other studies illustrated that astrocytes interact with microglia and modulate microglial phenotypes after TBI via exosome-containing microRNAs (miRNAs).[8,9]

Non-coding RNAs (ncRNAs) such as long non-coding RNA (lncRNA), miRNA, circular RNA (circRNA), and transfer RNA (tRNA), regulate biological processes of the cells.[10] Furthermore,

Received 7 June 2022; accepted 31 January 2023;
https://doi.org/10.1016/j.ymthe.2023.01.031.

[8]These authors contributed equally

Correspondence: Huaqiu Zhang, Department of Neurosurgery, Tongji Hospital of Tongji Medical College of Huazhong University of Science and Technology, Jiefang Avenue 1095, Wuhan 430030, China.
E-mail: zhanghq@tjh.tjmu.edu.cn

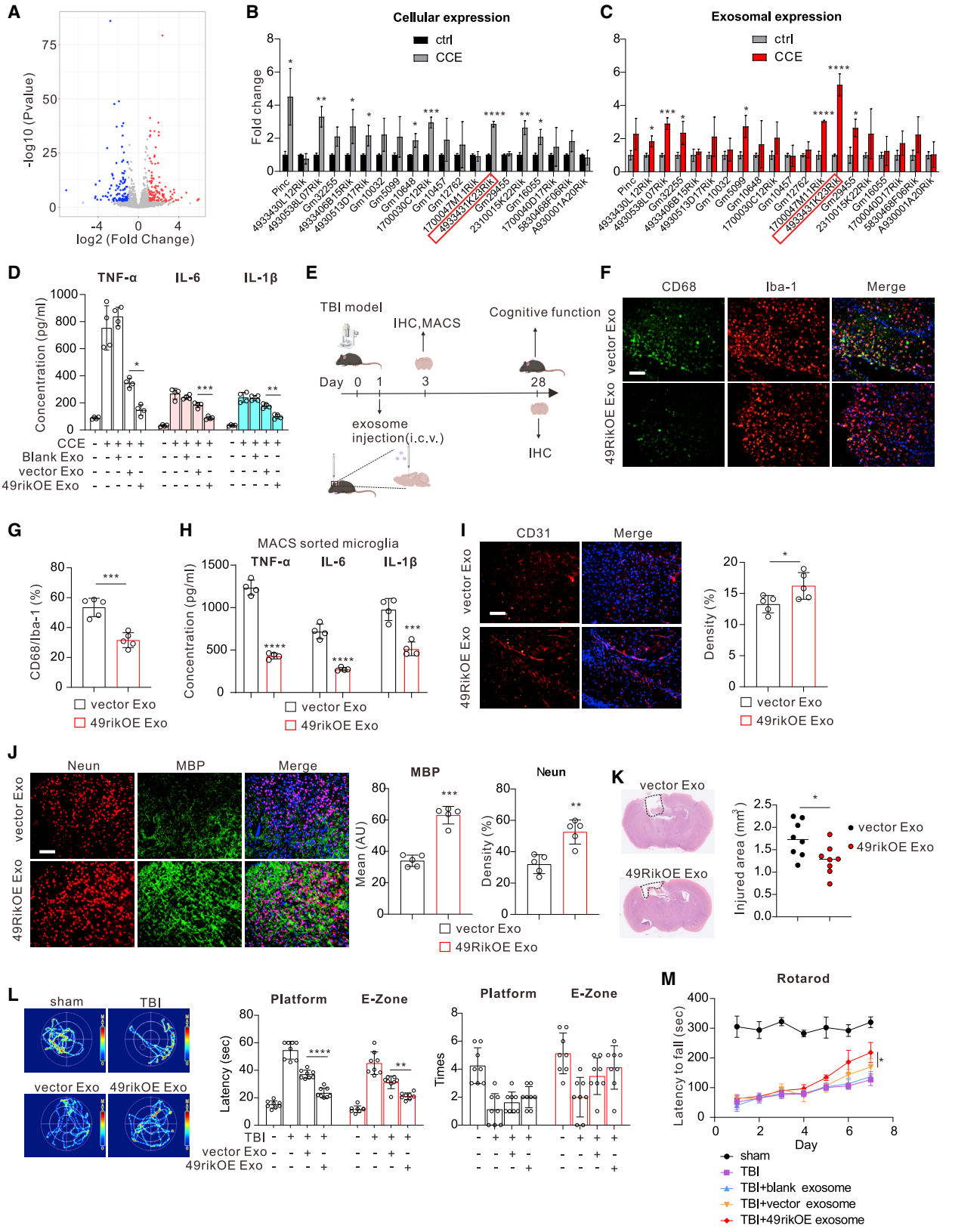

(legend on next page)

lncRNA interacts via "sponge-like" mechanisms to attach miRNA and thus prevents miRNA from binding to 3′ UTR of messenger RNA (mRNA) on the basis of specific sequence matching. This process has been recognized as important in the regulative methods of target mRNA.[11] However, there is a lack of research regarding exosomal lncRNA in post-TBI regulation, and the elucidation of its role in astrocyte-microglial interaction is required. Furthermore, the lncRNA/miRNA/mRNA regulative axis mechanism in TBI remains largely elusive.

Therefore, in this study, we proposed that astrocytes could regulate phenotypes of microglia via exosome-mediated lncRNA-miRNA-mRNA axes in TBI. Using transcriptomic sequencing and validation by qRT-PCR, we identified the specific lncRNA 4933431K23Rik/miR-10a-5p/E2F7 and TFAP2C axes post-TBI, which affect Smad7 expression in the microglia. Smad7 belongs to the TGF-β family and inhibits activation of the TGF-β and NF-κB signaling pathways.[12] Smad7 has been shown to have an important role in various diseases including autoimmune disease, inflammation-related disease, and cancers.[13] Previous studies demonstrated that Smad7 inhibits activation of NF-κB in an IκBα-dependent manner[14]; however its underlying mechanisms remain unknown. In addition, little is known about the role of Smad7 in TBI, particularly in terms of microglial properties. Here, we illustrated that up-regulation of microglial Smad7 alleviates microglial-induced neuroinflammation and chemotaxis and enhances phagocytosis activity, which promote recovery of cognitive function post-TBI. In addition, Smad7 directly binds to IκBα, resulting in a reduced level of ubiquitination and thus negatively regulating NF-κB activation.

Our study aimed to provided further insight into glial cell interaction post-TBI. Our findings could lead to using glia cell interaction as a promising therapeutic target for alleviating neuroinflammation and promoting positive clinical outcomes in patients with TBI.

RESULTS

Astrocyte-derived exosomal lncRNA 4933431K23Rik ameliorates microglial-induced neuroinflammation and improves cognitive function after TBI

Astrocytes and microglia are activated in TBI. According to single-cell sequencing data, microglia cells exhibit both pro-inflammatory and anti-inflammatory phenotype in TBI (Figures S1A and S1B). Therefore, simple lipopolysaccharide (LPS) stimulation cannot fully mimic TBI stimulation (Figure S1C). To better simulate TBI micro-environment stimulation, cerebral cortex extract (CCE) was used to stimulate the cells as previously described.[9,15] Using microglia as indicator, we observed that CCE successfully induced microglia displaying mixture inflammation phenotype (Figure S1C). Next, astrocytes were stimulated with cerebral cortex extract. After medium changing, the exosomes from the conditioned medium of the treated astrocytes were isolated and validated (Figures S2A–S2D). The exosomes were labeled with a specific membrane dye and applied to the microglial cells to reveal the efficient phagocytic effect of the exosomes on the microglia (Figures S2E–S2H).

To further investigate the regulating network of lncRNA-miRNA and to screen the potential targets, we performed lncRNA screening using RNA sequencing (RNA-seq) in cerebral cortex extract-treated astrocytes (see supplemental information for lncRNA sequencing [lncRNA-seq] datasets). We observed 152 up-regulated lncRNAs (Figure 1A) and selected the top 20 highest expressed lncRNAs for validation (Figure 1B). In addition, exosomes from CCE-treated astrocytes were examined for these 20 lncRNAs (Figure 1C). lncRNA 4933431K23Rik (49rik) was consistently more highly expressed by CCE-treated astrocytes (intracellularly) and in exosomes, and the increase in the expression level of 49rik was more predominant than that in the other candidates (Figures 1B and 1C). This indicates the potential role of lncRNA 49rik.

To our knowledge, there is no current research or information regarding the role of 49rik. Although 49rik is up-regulated after CCE stimulation, we primarily speculated that lncRNA 49rik may contribute to favorable pro-inflammatory progression. Therefore, microglial 49rik was knocked down by short hairpin RNA (shRNA), and CCE was used to induce TBI stimulation. Surprisingly, we observed that the 49rik knockdown effect on microglia induced an even higher level of pro-inflammatory signatures (Figures S3A–S3C). For further validation, lncRNA 49rik was knocked down and exosomes were collected to treat the microglia. Similarly, a decreased level of 49rik in the astrocyte exosomes also led to stronger pro-inflammation (Figure S3D). These data suggest that exosomal 49rik from astrocytes has an attenuation role rather than a pro-inflammatory role in post-TBI microglial activation.

Figure 1. Astrocyte-derived exosomes ameliorate microglial-induced neuroinflammation and improve cognitive function after traumatic brain injury (TBI) via long non-coding (lnc)RNA 4933431K23Rik

(A) Volcano plot shows the differentially expressed genes of astrocytes after 6 h cerebral cortex extract (CCE, 5 μg/mL) treatment. (B) The top 20 up-regulated lncRNAs were examined using reverse transcription-quantitative polymerase chain reaction (qRT-PCR) in astrocytes after 6 h CCE (5 μg/mL) treatment. (C) Exosomes from astrocytes were detected for the same lncRNAs as that noted in (B). (D) Exosomes were isolated from supernatant of astrocytes (Blank Exo); vector-transfected astrocytes with CCE treatment (vector Exo) and lncRNA 4933431K23Rik overexpressed astrocyte after CCE treatment (49rikOE Exo). Exosomes were then applied to microglia with or without CCE treatment (5 μg/mL) as stimulation. Pro-inflammatory factors were examined using ELISA. (E–M) Schematic figure illustrates that mice were intraventricularly (i.c.v.) administrated with exosomes (vector Exo or 49RikOE Exo) 1 day after traumatic brain injury (TBI) (E). (F) TBI brains were collected on day 3 for CD68 (green) and Iba-1 (green) staining. DAPI (blue) was used as nuclei labeling. Scale bar, 50 μm. (G) Quantification of CD68 and Iba-1 double-positive cells normalized to DAPI numbers. (H) TBI brains were collected on day 3 for microglia isolation using MACS. Cytokines of isolated microglia were determined using ELISA. (I and J) TBI brains were collected on day 3 post-TBI and used for vessels (CD31, red, I)/neuronal (Neun, red, J)/myelin (MBP, green, J) immunofluorescence staining. Scale bar, 50 μm. (K–M) TBI brains were collected on day 28 for hematoxylin and eosin (H&E) staining, and Morris water maze (L) and rotarod (M) were used to determine the cognitive activity and motor capability, respectively. *$p < 0.05$, **$p < 0.01$, ***$p < 0.001$, and ****$p < 0.0001$. Data are presented as mean ± SD.

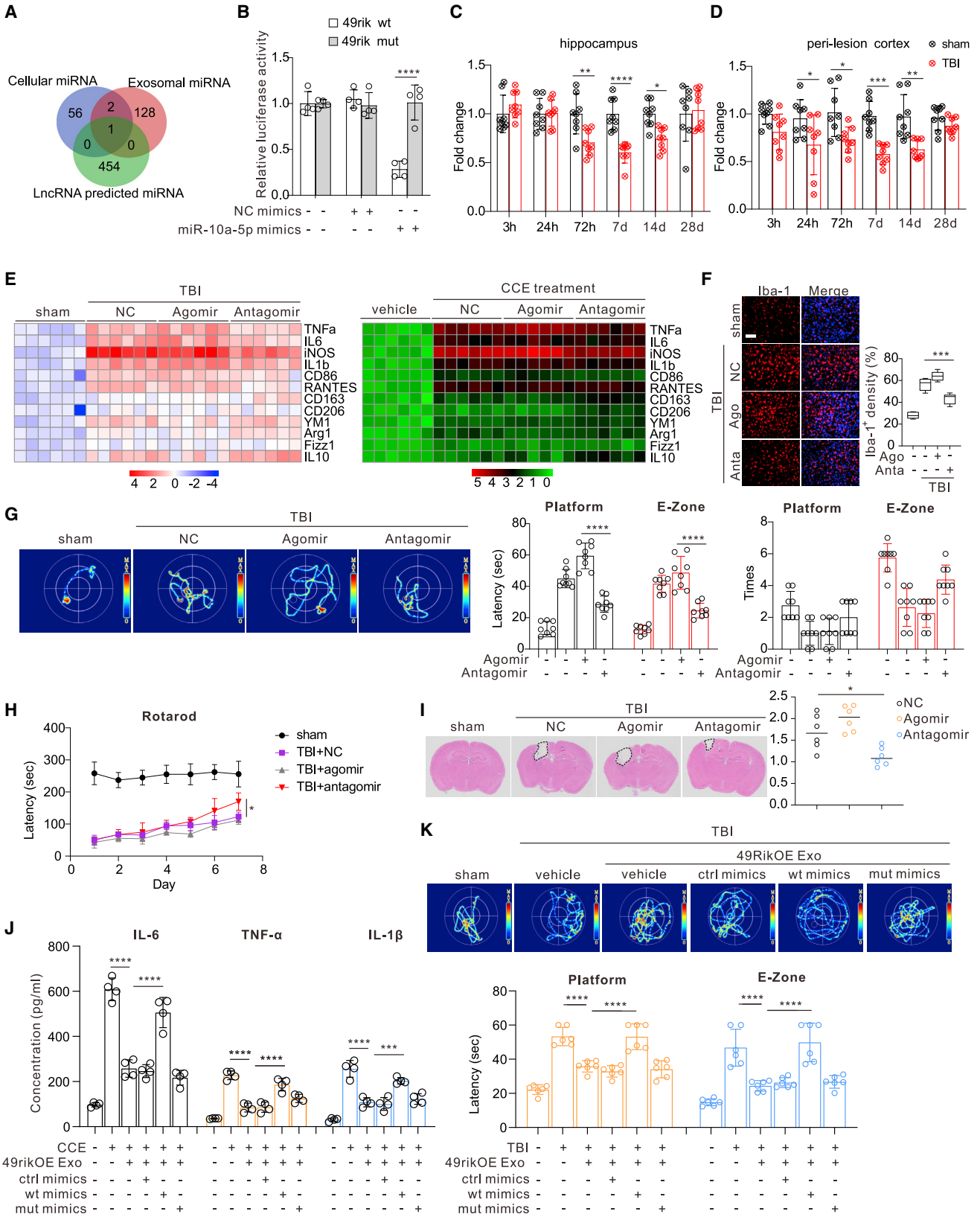

(legend on next page)

To further determine the effect of exosomal lncRNA 49rik on microglial pro-inflammatory properties, 49rik was overexpressed by astrocytes combined with CCE treatment. After a medium change, exosomes were isolated from astrocyte-conditioned medium (ast CM) and applied to the microglia. We observed that 49rik overexpression exosomes efficiently attenuated CCE-induced pro-inflammatory factor (tumor necrosis factor-α [TNF-α], interleukin [IL]-6, and IL-1β) release in microglia *in vitro* (Figure 1D). To prove this *in vivo*, TBI model was conducted, and exosomes 49rik overexpression exosomes were intraventricularly (i.c.v.) applied to the TBI mice (Figure 1E). The biological distribution and microglial targeting of exosomes were verified by fluorescence labeled exosome delivery. As shown in Figure S4A, approximately 95% of exosomes were engulfed by microglial cells either in peri-lesion cortex or hippocampus (Figure S4A). We first histologically evaluate the effect of exosomal 49rik on the brain after TBI. Staining results show that the exosomal 49rik significantly decreased pro-inflammatory microglial cells defined by CD68 (Figures 1F and 1G). Furthermore, microglia were isolated from the exosome treated TBI brains by magnetic activated cell sorting (MACS) as our previous methods.[16,17] We examined the pro-inflammatory cytokines released from these MACS-sorted cells. As expected, exosomal 49rik attenuated microglia derived TNF-α, IL-6, and IL-1β release (Figure 1H). Moreover, we determined the protective role of exosomal 49rik on neurovascular unit. Indeed, exosomal 49rik treatment increased the densities of neurovascular units in the peri-lesion cortex of TBI mice (Figures 1I and 1J). Lesion volumes were evaluated using hematoxylin and eosin (H&E) staining. We observed remarkably smaller lesion volumes in brains treated with exosomal 49rik (Figure 1K).

Accumulative evidence has shown that neuroinflammation impedes cognitive behavior recovery post-TBI. Here, we also determined the impact of exosomal 49rik on post-TBI cognitive function. Consistent with our observation regarding neuroinflammation, exosomal 49rik also notably improved the recovery of post-TBI cognitive function as assessed using the Morris water maze (MWM) (Figure 1L). Furthermore, motor capability was evaluated; similar to the results of MWM, exosomal 49rik significantly improved the motor performance as determined using the Rotarod Assay (Figure 1M). To further verify that the curative effect of exosomal 49rik is based on microglia, microglial cells were depleted in the mouse brain using clodronate liposome as previously described,[18] and exosomal 49rik was applied (Figure S4B). We found that microglia depletion can remarkably impaired the treating effect of exosomal 49rik (Figures S4C and S4D), indicating the microglia specific role in the exosomal 49rik treatment.

Taken together, our data illustrated that TBI stimulates astrocytes to release lncRNA 49rik which alleviates microglial-associated neuroinflammation and improves post-TBI recovery.

lncRNA 4933431K23Rik attenuates microglial activation and improves neurological function through sponging of miR-10a-5p

To further investigate the regulating mechanisms of lncRNA 49rik, CCE-treated astrocyte cellular miRNA and exosomal miRNA sequencing were performed to identify target miRNA (see supplemental information for miRNA sequencing [miRNA-seq] datasets). Furthermore, the down-regulated miRNA from these two datasets was analyzed combined with lncRNA 49rik predicted targets (using the miRANDA database [http://www.microrna.org/microrna/home.do]), as previously described.[18] As shown in Figure 2A, miR-10a-5p as the predicted target for lncRNA 49rik that is down-regulated both in the cellular and exosomal levels of astrocytes, indicates its potential regulating capacity for lncRNA 49rik-mediated post-TBI recovery. To validate that lncRNA 49rik directly interacts with miR-10a-5p, we transfected the mutant 49rik vector with unmatched sequence to miR-10a-5p into cells together with miR-10a-5p and observed significant cellular luciferase signal decrease (Figure 2B), indicating the specific matching between the lncRNA 49rik and miR-10a-5p.

Next, we determined the expression pattern and impact of miR-10a-5p in TBI. The expression pattern of miR-10a-5p in the TBI models among different days post-TBI were assessed using qRT-PCR. We

Figure 2. Long non-coding RNA (lncRNA) 4933431K23Rik attenuated post-traumatic brain injury (TBI) microglial activation and improved neurological function through sponging of miR-10a-5p

(A) RNA sequencing was used to determine the microRNA (miRNA) level changes after cerebral cortex extract (CCE; 5 μg/mL) treatment. The Venn diagram depicts the overlap among down-regulated miRNAs in astrocytes and exosomes, and miRNAs associated with long non-coding RNA 4933431K23Rik were predicted by miRANDA software. (B) Luciferase assay shows sequence-specific binding of lncRNA 4933431K23Rik (49rik) and miR-10a-5p. (C and D) Expression level of miR-10a-5p in murine hippocampus (C) and peri-lesion cortex (D) post-TBI at different time points. (E) TBI mice intraventricularly treated with negative control agomir plus antagomir (NC), negative control antagomir plus miR-10a-5p agomir (agomir), or negative control agomir plus miR-10a-5p antagomir (antagomir) (left). Microglial cells were treated with CCE (5 μg/mL) in the presence of negative controls (NC) or miR-10a-5p agomir or antagomir (right). Gene expression of pro- and anti-inflammatory signatures were examined in TBI mice brains using qRT-PCR; the heatmap shows the corresponding changes. (F and H) TBI mice intraventricularly treated with negative control agomir plus antagomir (NC), negative control antagomir plus miR-10a-5p agomir (agomir), or negative control agomir plus miR-10a-5p antagomir (antagomir) were examined for microglia density using immunofluorescence staining (Iba-1, red; scale bar, 50 μm), cognitive behavior using the Morris water maze (representative figure of training phase in G), and movement ability using the rotarod assay (H). (I) Representative figures of hematoxylin and eosin (H&E) staining indicate lesion volume changes of TBI mice after intraventricularly negative control antagomir (NC), miR-10a-5p agomir or antagomir treatment. (J) Microglial cells were treated with exosomes isolated from lncRNA 4933431K23Rik-overexpressed astrocytes (49ridOE Exo) combined with CCE (5 μg/mL) treatment. Control miRNA mimics (ctrl mimics), miR-10a-5p mimics (WT mimics), and sequence mutant miR-10a-5p mimics (mut mimics) were also added to the cells. ELISA detected the level of pro-inflammatory factors in the supernatant. (K) TBI mice were intraventricularly treated with exosomes and miRNA mimics as described in (J). Morris water maze results show the cognitive behavior of TBI mice after corresponding treatment. *$p < 0.05$, **$p < 0.01$, ***$p < 0.001$, and ****$p < 0.0001$. Data are presented as mean ± SD.

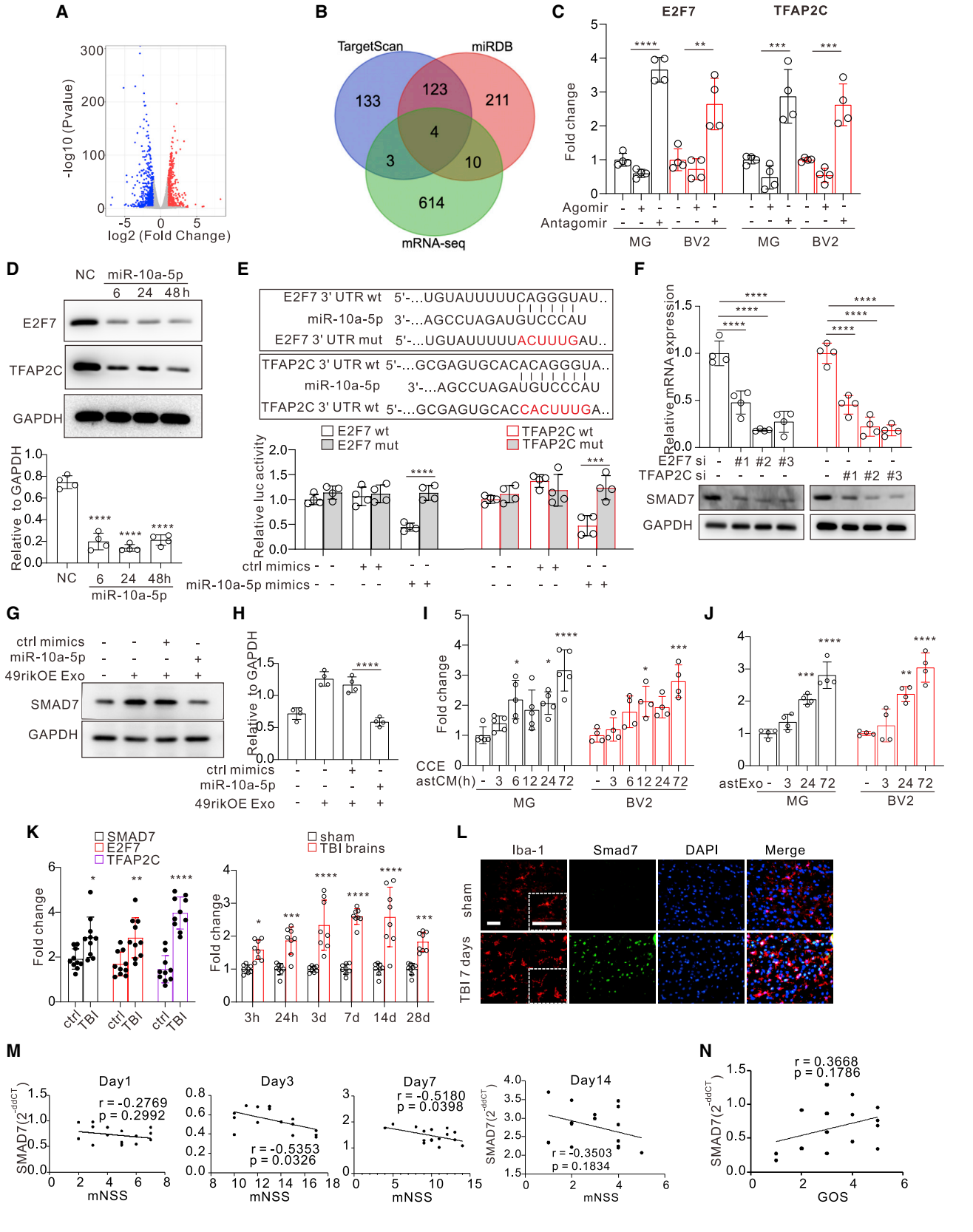

(legend on next page)

found that miR-10a-5p decreased in both peri-lesion cortex and hippocampus of TBI brains (Figures 2C and 2D). To further understand the regulative role of miR-10a-5p, we characterized the impact of miR-10a-5p in TBI-induced neuroinflammation via qRT-PCR. We indeed observed the attenuation of pro-inflammatory signatures (when applied with miR-10a-5p antagomir) that could specifically down-regulate the miR-10a-5p level in a TBI mouse model (Figure 2E, left) and in an *in vitro* TBI model (Figure 2E, right). Furthermore, notably fewer infiltrating microglia were found in the miR-10a-5p antagomir-treated TBI mice compared with those in the negative control (NC) antagomir group (Figure 2F). In addition, we evaluated the effect of miR-10a-5p on neuronal function recovery post-TBI. The MWM results showed significant improvement in the cognitive function of TBI mice after miR-10a-5p antagomir treatment (Figure 2G). Similarly, the Rotarod Assay illustrated that miR-10a-5p antagomir promoted motor performance of TBI mice (Figure 2H). To further demonstrate the protective role of miR-10a-5p inhibition, we measured the lesion area of a TBI mouse model and found a notably smaller lesion area in the miR-10a-5p antagomir treatment TBI group (Figure 2I). Besides, we testified the effect of miR-10a-5p inhibition in human microglial cell (HMC-3). Similar to murine microglia, miR-10a-5p suppression also efficiently attenuate CCE induced elevation of pro-inflammatory markers expression (Figures S5A and S5B).

Our hypothesis was that lncRNA 49rik regulates the microglia phenotype and the outcome of TBI via sponging of miR-10a-5p. We first validated this by detecting the pro-inflammatory factors of CCE-treated microglia and adding exosomes from lncRNA 49rik-overexpressed astrocytes combined with miR-10a-5p mimics. We again observed a remarkable decrease of microglial-released pro-inflammatory cytokines after adding the exosomes from the lncRNA 49rik-overexpressed astrocyte. However, this attenuation could be reversed in the presence of miR-10a-5p mimics (Figure 2J). In addition, the results of the MWM showed that miR-10a-5p efficiently reversed lncRNA 49rik-induced cognitive recovery post-TBI (Figure 2K). In summary, these results demonstrated that lncRNA 4933431K23Rik sponges miR-10a-5p and thus attenuates microglial activation and improves neurological function post-TBI.

4933431K23Rik sponging of miR-10a-5p enhanced SMAD7 expression through direct regulation of transcription factors E2F7 and TFAP2C

As lncRNA/miRNA mainly participates in mRNA regulation, we further investigated the actual functional downstream mRNA. mRNA sequencing (mRNA-seq) was first performed on CCE-treated astrocytes (Figure 3A) (see supplemental information for mRNA-seq datasets), and we then analyzed the up-regulated mRNA genes combined with miR-10a-5p potentially regulated genes using two different prediction software programs (TargetScan [https://www.targetscan.org/mmu_80/], miRDB [https://mirdb.org]) (Figure 3B). Among the four identified mRNAs, we characterized E2F7 and TFAP2C as potentially direct targets of miR-10a-5p. To determine E2F7 and TFAP2C as direct functional targets of lncRNA 49rik/miR-10a-5p axis, we first transfected microglial cells with miR-10a-5p agomir or antagomir. Then, we assessed the mRNA levels of E2F7 and TFAP2C using qRT-PCR. As expected, miR-10a-5p suppressed the mRNA expression of E2F7 and TFAP2C (Figure 3C). Furthermore, this regulation was confirmed using western blot analysis of protein levels (Figure 3D). To further verify the direct regulating effect of miR-10a-5p toward E2F7 and TFAP2C, luciferase assay showed that miR-10a-5p specifically binds to E2F7 and TFAP2C (Figure 3E). As TFAP2C and E2F7 are both transcription factors that regulate various genes' expressions, we speculated that these two transcription factors could affect the downstream genes that modulate microglial phenotypes. Therefore, we performed meta-analysis of TFAP2C and E2F7 potentially regulated genes. Using our mRNA-seq data, we then identified that Smad7 may be the most probable target (see Figure S6). In addition, we have also observed that miR-10a-5p inhibition resulted in SMAD7 up-regulation in human microglial cells (Figure S5C). Little is known about the effect of Smad7 on TBI, particularly about the effect on the microglia. Before we investigated the effects of Smad7 on TBI and microglia, we first verified whether E2F7 and TFAP2C could directly regulate the expression of SMAD7. E2F7 and TFAP2C were silenced on microglial cells (BV-2), respectively, and the protein expression of SMAD7 was down-regulated (Figure 3F). In addition, we confirmed that the lncRNA 49rik-induced Smad7 up-regulation could be attenuated by miR-10a-5p (Figures 3G and 3H). These data illustrated that

Figure 3. 4933431K23Rik sponging miR-10a-5p enhanced SMAD7 expression through regulating transcription factors E2F7 and TFAP2C

(A) Volcano plot denotes differential messenger RNAs (mRNAs) of astrocytes after cerebral cortex extract (CCE; 5 μg/mL) treatment. (B) Venn diagram indicates overlap among predicted miR-10a-5p target mRNAs and up-regulated mRNA in (A). (C) Primary microglia (MG) and cell line (BV-2) were treated with control agomir or antagomir, miR-10a-5p agomir or antagomir, respectively, and gene expression levels of E2F7 and TFAP2C were examined using qRT-PCR. (D) BV-2 cells were treated with control mimics (NC) for 48 h and miR-10a-5p mimics for different times, and protein levels of E2F7 and TFAP2C were detected using western blot. (E) Luciferase assay indicates specific binding among miR-10a-5p, E2F7, and TFAP2C. (F) BV-2 microglial cells were silenced for E2F7 or TFAP2C by siRNAs. SMAD7 expression was measured using qRT-PCR (up) and western blot (down). (G and H) Protein expression of microglial SMAD7 after treatment with exosomes isolated from long non-coding RNA (lncRNA) 4933431K23Rik-overexpressed astrocytes (49rikOE Exo) combined with control or miR-10a-5p mimics. (I) Microglial SMAD7 mRNA level changes after treatment with CCE-stimulating astrocyte-conditioned medium (CCE ast CM) for different time points. (J) Microglial SMAD7 mRNA level changes after treatment with exosomes isolated from CCE-stimulating astrocyte-conditioned medium (astExo) for different time points. (K) Gene expression of SMAD7, E2F7, and TFAP2C in mice brains 3 days post-traumatic brain injury (TBI) (left) and mRNA level of SMAD7 in distinct time points post-TBI (right). (L) Representative figures of SMAD7 protein expression (green) on microglia (red) post TBI via immunofluorescence staining. Scale bar, 50 μm. (M) The correlation between mNSS (modified neurological severity scores) of TBI mice and SMAD7 mRNA brain levels. (N) The correlation between GOS (Glasgow Outcome Scale) scores of patients with TBI and the SMAD7 mRNA expression in resected traumatic tissues. $^{*}p < 0.05$, $^{**}p < 0.01$, $^{***}p < 0.001$, and $^{****}p < 0.0001$. Data are presented as mean ± SD.

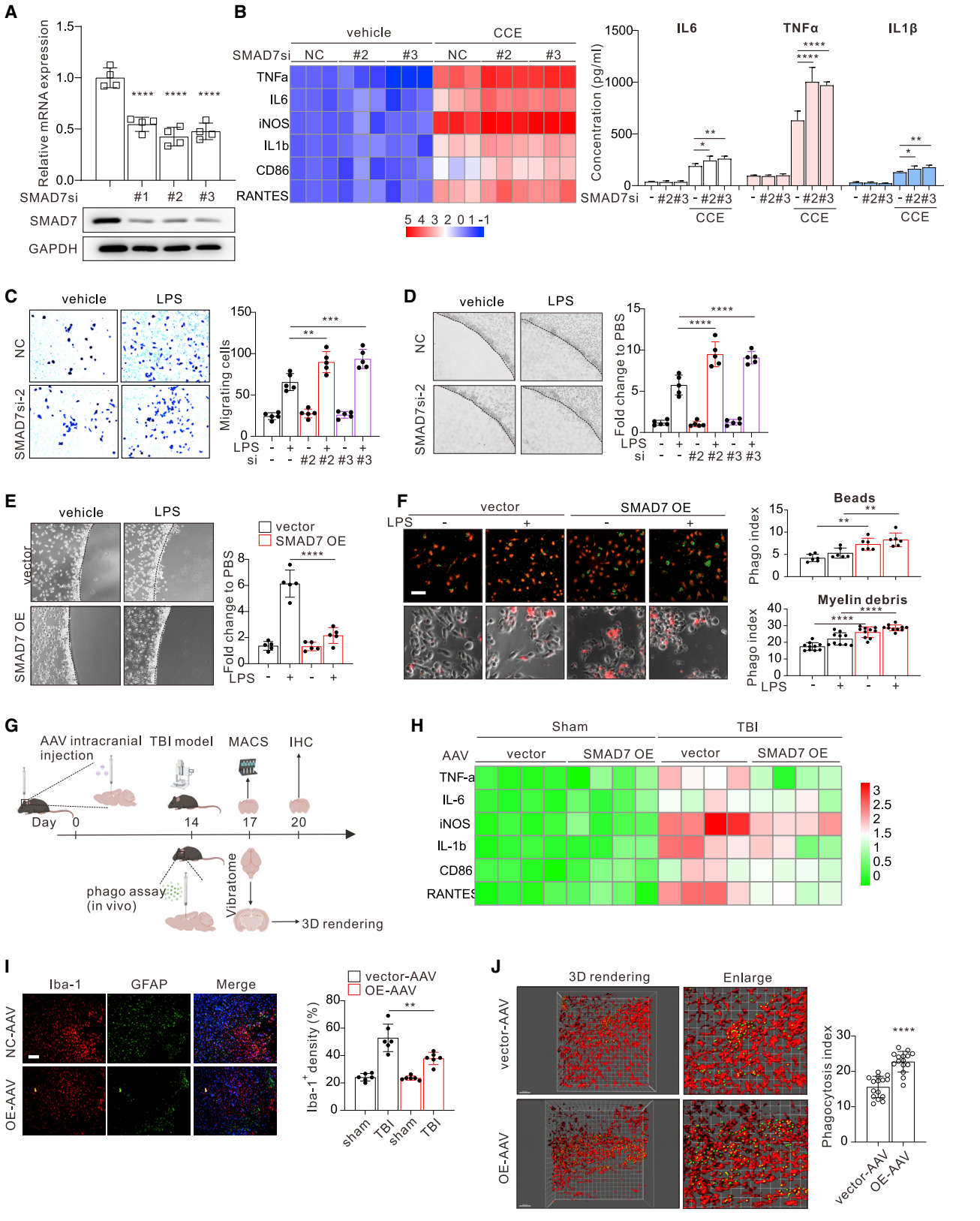

(legend on next page)

the lncRNA 49rik/miR-10a-5p/E2F7&TFAP2C axis regulates Smad7 expression in the microglia. These results could explain our previous observations.

Next, we assessed the expression pattern of microglial Smad7 after treating them with an astrocyte-conditioned medium (Figure 3I) and exosomes (ast Exo) (Figure 3J), respectively. We observed increased Smad7 expression in a time-dependent manner (Figures 3I and 3J). Furthermore, we observed higher expression of E2F7, TFAP2C, and SMAD7 in TBI mice, among which SMAD7 was expressed differentially for various time points post-TBI (Figure 3K). The co-localization expression of SMAD7 and microglia was also found in the TBI brains (Figure 3L). In addition, we analyzed the correlation between SMAD7 expression and the modified neurological severity scores (mNSSs) of TBI mice in different post-TBI time points and found a negative correlation on days 3 and 7 post-TBI (Figure 3M). Even though the difference was not significant, there was a tendency for positive correlation between the SMAD7 expression and Glasgow Outcome Scale (GOS) scores of patients with TBI (Figure 3N). Taken together, our data suggest that the lncRNA 4933431K23Rik sponging of miR-10a-5p increases the SMAD7 expression in TBI.

SMAD7 affected TBI-induced microglial activation, including phenotype switch and chemotaxis and phagocytosis activity

SMAD7 is a member of the TGF-β signaling family which negatively regulates its activation. Through a non-canonical pathway, SMAD7 has an important role in inhibiting NF-κB and regulating cellular function under disease conditions.[19] However, there is lack of knowledge of the impact of SMAD7 on microglial properties in TBI. To systematically study the function of SMAD7 on microglia, first, the microglial cells were silenced with silencing RNA (siRNA) and the efficiency was confirmed using both qRT-PCR and western blot (Figure 4A). Then, pro-inflammatory-related signatures of the SMAD7-silencing microglia under CCE stimulation were detected; a notable increase of these genes was observed (left, Figure 4B). Moreover, the up-regulation of pro-inflammatory cytokines by SMAD7 silencing were validated using ELISA (Figure 4B, right). Transwell and agarose spot assays were used to determine microglial migrating and chemotaxis activity after SMAD7 silencing. We found that SMAD7 silencing significantly amplified the migrating (Figure 4C) and chemotaxis activity (Figure 4D) of microglia. Conversely, SMAD7 overexpression led to remarkably less chemotaxis capability (Figure 4E). Next, we assessed the influence of SMAD7 on microglial phagocytosis activity by applying fluorescence phagocytosis beads (Figure 4F, up) or fluorescence labeled myelin (Figure 4F, down) to the SMAD7-overexpressed microglia. The microglial phagocytosis activity toward beads or myelin was remarkably enhanced by SMAD7 overexpression (Figure 4F).

To investigate the effect of SMAD7 on microglia properties *in vivo*, we developed the pAAV-Cx3cr1 promoter-3xFLAG-P2A-SMAD7-mCherry-tWPA adeno-associated virus (AAV) to specifically overexpress SMAD7 on the microglia *in vivo* (Figure S7). The vector AAV or SMAD7 overexpression AAV were inoculated into mice brains for 14 days prior to TBI model (Figure 4G). We then evaluated the pro-inflammatory factors of magnetic-activated cell sorting sorted microglia 3 days post-TBI using qRT-PCR and determined the microglia infiltration level on day 7 post-TBI. We found that SMAD7 overexpression on microglia drastically attenuated microglial pro-inflammatory factor expression (Figure 4H) and infiltration (Figure 4I). Furthermore, we measured the phagocytosis activity *in vivo* by injecting fluorescence labeled beads prior to confocal microscope scanning and IMARS three-dimensional (3D) reconstruction (Figure 4J). Similar to our *in vitro* data, microglial SMAD7 overexpression *in vivo* also showed enhanced phagocytosis activity (Figure 4J). Taken together, these results demonstrated that SMAD7 affects the microglial phenotype switch, migration, chemotaxis, and phagocytosis activity post-TBI.

Microglial-specific SMAD7 overexpression improved recovery of cognitive function, neurovascular unit, and blood brain barrier (BBB) integrity post-TBI

Our results revealed that SMAD7 attenuates microglial pro-inflammatory phenotype and infiltration and increases post-TBI debris clearance (phagocytosis). To continue our investigation, we decided to determine whether this SMAD7 affects TBI recovery. Similar to our previous description, microglial-specific SMAD7 overexpression AAV was injected into mice brains; the TBI model was induced 14 days after AAV injection. Subsequently, behavior tests (MWMs and

Figure 4. SMAD7 affected traumatic brain injury (TBI)-induced microglial activation including phenotype switch, chemotaxis, and phagocytosis activity

(A) Protein expression of SMAD7 on microglial cells after transfection with SMAD7 silencing RNA (siRNA). (B) SMAD7-silenced microglia (#2, #3) were treated with cerebral cortex extract (CCE; 5 μg/mL), and pro-inflammatory signatures were checked using qRT-PCR and ELISA. Heatmap indicates the changes of corresponding genes (right). Bar graph indicates the protein level in the supernatant. (C and D) SMAD7-silenced microglia (#2, #3) were treated with lipopolysaccharide (LPS) (100 ng/mL). The migrating activity was determined using Transwell assay (C) with quantification on the right. The chemotaxis activity was determined using agarose spot assay (D) with quantification on the right. (E) SMAD7-overexpressed microglia (SMAD7 OE) were treated with LPS (100 ng/mL), and the chemotaxis activity was determined using agarose spot assay, with quantification on the right. (F) The representative figures depict the phagocytosis capacity of vector-transfected (NC) and SMAD7-overexpressed (SMAD7 OE) microglia, evaluating the engulfing beads (up, green) and fluorescence myelin debris (down, red). Scale bar, 50 μm. (G–J) Schematic figure illustrates the intracranial injection of mice with Cx3cr1-Smad7 overexpression adeno-associated virus (AAV) to specifically increase the Smad7 level in microglia *in vivo,* and the traumatic brain injury (TBI) model was subsequently generated on day 14 (G). Three days after TBI, microglia were isolated using magnetic-activated cell sorting (MACS). The heatmap shows pro- and anti-inflammatory signature changes (H). After 14 days post-TBI, the brain slices were examined for Iba-1 (red) and glial fibrillary acidic protein (GFAP) (green). Scale bar, 100 μm (I). The representative 3D rendering shows the microglial phagocytosis capacity *in vivo*. The ratio of engulfed beads (green) within microglial cellular volume (red) is quantified on the right (J). *$p < 0.05$, **$p < 0.01$, ***$p < 0.001$, ****$p < 0.0001$. Data are presented as mean ± SD.

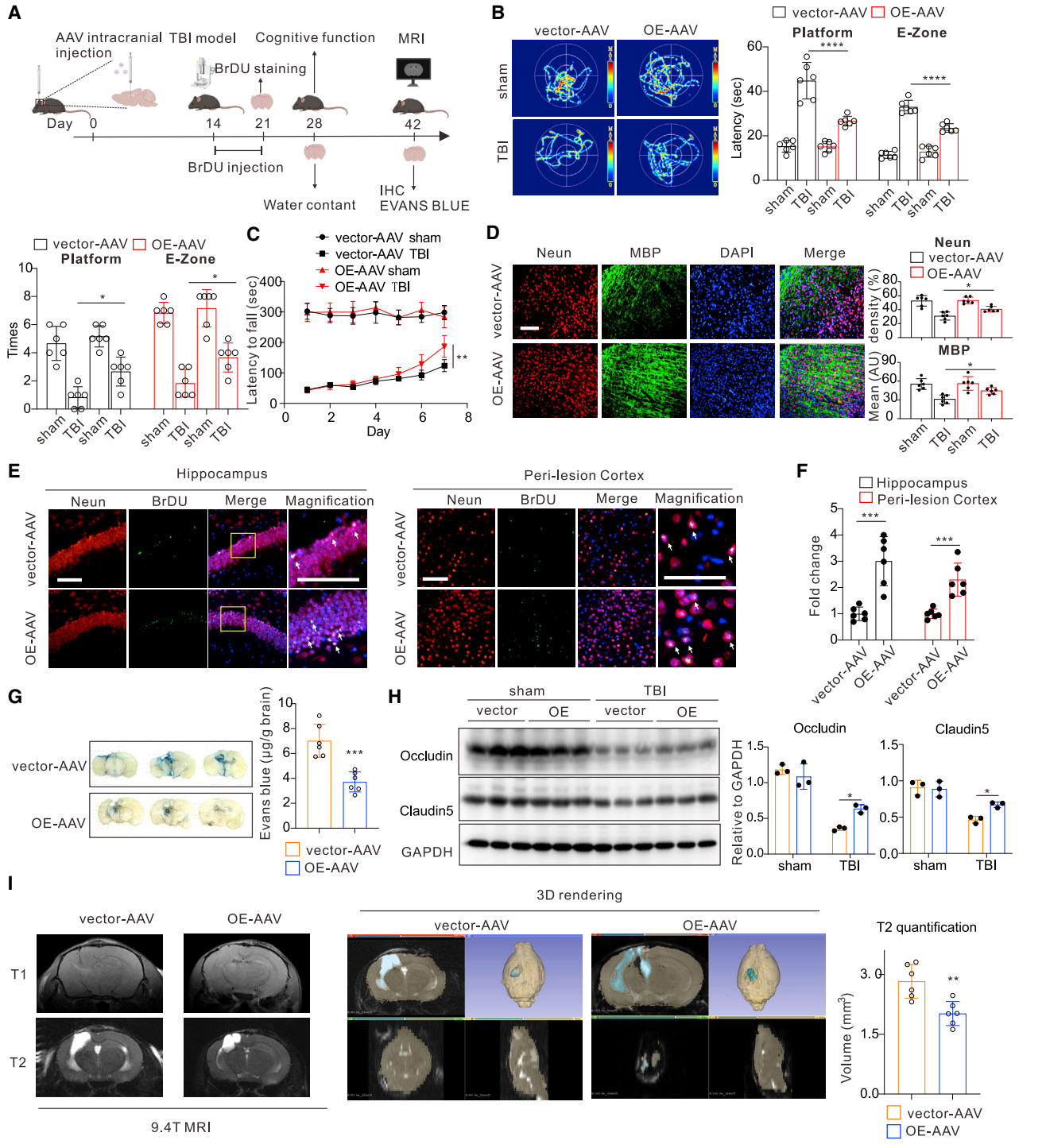

(legend on next page)

rotarod assays) were performed on day 14 post-TBI (Figure 5A). Similar to lncRNA 49rik-overexpressed exosomes treatment, microglial SMAD7 overexpression promoted the behavior of TBI mice (Figures 5B and 5C). Neuronal structure recovery has been shown as a hallmark for improvement of TBI outcome; therefore, in our study we also stained the brain slices for neurons and myelin (oligodendrocytes). We found that SMAD7 overexpression also increased the density of these neuronal structure units (Figure 5D). To investigate the effect of microglial SMAD7 overexpression on neurogenesis post-TBI, 5-bromo-2′-deoxyuridine (BrDU) was used. Indeed, microglial SMAD7 overexpression resulted in increased level of neurogenesis in both hippocampus and peri-lesion cortex from TBI mice (Figures 5E and 5F). In addition, recovery of the BBB integrity was found in the SMAD7 overexpression TBI mice determined using Evans blue assay and detection of tight junctions (Figures 5G and 5H).

To comprehensively evaluate the recovery in TBI lesions, SMAD7 overexpression TBI mice were examined using 9.4-T MRI (9.4-T uMRI) for T1 and T2 structural scanning (Figure 5I). The lesion volumes on the T2 phase were analyzed by 3D reconstruction using a 3D slicer (Figure 5I). SMAD7 overexpression on microglia resulted in significantly smaller lesion volumes post-TBI. These findings were also confirmed via H&E staining (Figure 5J).

As our ultimate goal is to translate the experimental findings to clinical usage, we then selected and verify the treatment efficiency of asiaticoside (Ats), a previously described SMAD7 activator,[20–22] in TBI. As shown in Figure S8A, asiaticoside efficiently induced elevation of SMAD7 expression in microglia *in vitro* and cortex tissue from Ats-treated TBI mice expressed higher level of SMAD7. In addition, to verify its protective role in TBI, Ats was applied to the TBI mice, and we observed the significant cognitive improvement and improved level of neurogenesis of TBI mice treated with Ats compared with vehicle groups (Figures S8C and S8D).

Taken together, our results illustrated that microglial SMAD7 overexpression alleviated post-TBI neuroinflammation, improve neurogenesis as well as integrity of neurovascular structures, and promote recovery of cognitive functions.

SMAD7 attenuated NF-κB cascade activation through competitive inhibiting K48 ubiquitination of negative regulator Iκbα

NF-κB signaling has a pivotal role in regulating microglia/macrophage activation and can be considered a central regulative pathway in the phenotype switch.[23,24] SMAD7 has been demonstrated as capable of inhibiting the NF-κB signaling pathway by affecting Iκbα expression; however, the mechanisms behind this inhibition remain unclear. Our data revealed that SMAD7 affected microglial activation; therefore, we proposed that SMAD7 may regulate microglial function in TBI by inhibiting NF-κB signaling. To investigate this proposal, we first determined the expression level of NF-κB P65 and NF-κB P50 in the nuclei after SMAD7 overexpression, and we indeed observed that nuclei translocation of NF-κB P65 and NF-κB P50 was attenuated (Figure 6A, left). Furthermore, SMAD7 overexpression was found to increase the negative regulator IκBα expression in cell cytoplasm (Figure 6A, right). We also verified this in the *in vivo* SMAD7 overexpression induced by AAV (Figure 6B). These results indicate the inhibition effect of SMAD7 on NF-κB activation.

As we and other researchers revealed that SMAD7 was capable of enhancing the expression of IκBα, and IκBα is generally ubiquitination and degradation during the NF-κB signaling activation process,[25] we presumed that SMAD7 may regulate the ubiquitination process of IκBα and thus increase its expression. Therefore, we performed immunoprecipitation (IP) on microglia to examine the physical interaction between SMAD7 and IκBα. Surprisingly, we found that SMAD7 directly interacted with IκBα (Figure 6C). Furthermore, the IP complex (SMAD7 antibody captured) was detected for K48 ubiquitination, and the IP expression at 39 kDa was significantly inhibited by SMAD7 overexpression, indicating the protective role of SMAD7 on IκBα K48 ubiquitination. To further demonstrate this role, we used cycloheximide (CHX) and SMAD7 overexpression to successfully alleviate IκBα degradation (Figure 6D). Taken together, our results suggest that SMAD7 directly binds to IκBα and inhibits K48 ubiquitination, protecting its degradation and thus inhibiting NF-κB signaling activation (Figure 6E).

Figure 5. Microglial-specific SMAD7 overexpression improved recovery of cognitive function, neurovascular unit, and blood-brain barrier (BBB) integrity

(A) Schematic figure illustrates the intracranial injection of mice with Cx3cr1-SMAD7 overexpression adeno-associated virus (AAV) to specifically increase the SMAD7 level in microglia *in vivo*. Fourteen days post-injection, the traumatic brain injury (TBI) model was conducted, and cognitive function was examined on day 14 post-TBI. The structural changes were assessed on day 28 post-TBI. (B) Morris water maze was used to examine cognitive behavior of control vector AAV (vector-AAV) or SMAD7-overexpressed AAV (OE-AAV) treated TBI mice. Latency of finding the target and effective crossing times were recorded and quantified. (C) Rotarod assay was used to determine the movement ability of control vector AAV (vector-AAV) or SMAD7-overexpressed AAV (OE-AAV) treated TBI mice. Latency to fall was recorded and quantified. (D) TBI brain slices were used for assessing neuronal (Neun, red) and myelin density (Mbp, green). (E) BrDU was injected after conducting TBI model for 7 days. Specimens of TBI brains were assessed for neurogenesis using Neun (red) and BrDU (green) staining. The white arrows indicate double staining of Neun and BrDU. (F) Quantification of Neun and BrDU double-positive cells. (G) Evans blue assay shows BBB integrity changes between control vector AAV (vector-AAV) or SMAD7-overexpressed AAV (OE-AAV) treated TBI mice. (H) Western blot indicates tight junction protein expression of claudin-5 in the control vector AAV (vector-AAV) or SMAD7-overexpressed AAV (OE-AAV) treated TBI peri-lesion cortex tissue. (I) MRI (9.4 T) shows the traumatic lesion between control vector AAV (vector-AAV) or SMAD7-overexpressed AAV (OE-AAV) treated TBI mice (OE-AAV). The 3D rendering shows the T2 sequence. (I) Hematoxylin and eosin (H&E) staining suggests lesion volume of vector (vector) and SMAD7-overexpressed TBI mice (SMAD7 OE). *$p < 0.05$, **$p < 0.01$, ***$p < 0.001$, and ****$p < 0.0001$. Data are presented as mean ± SD.

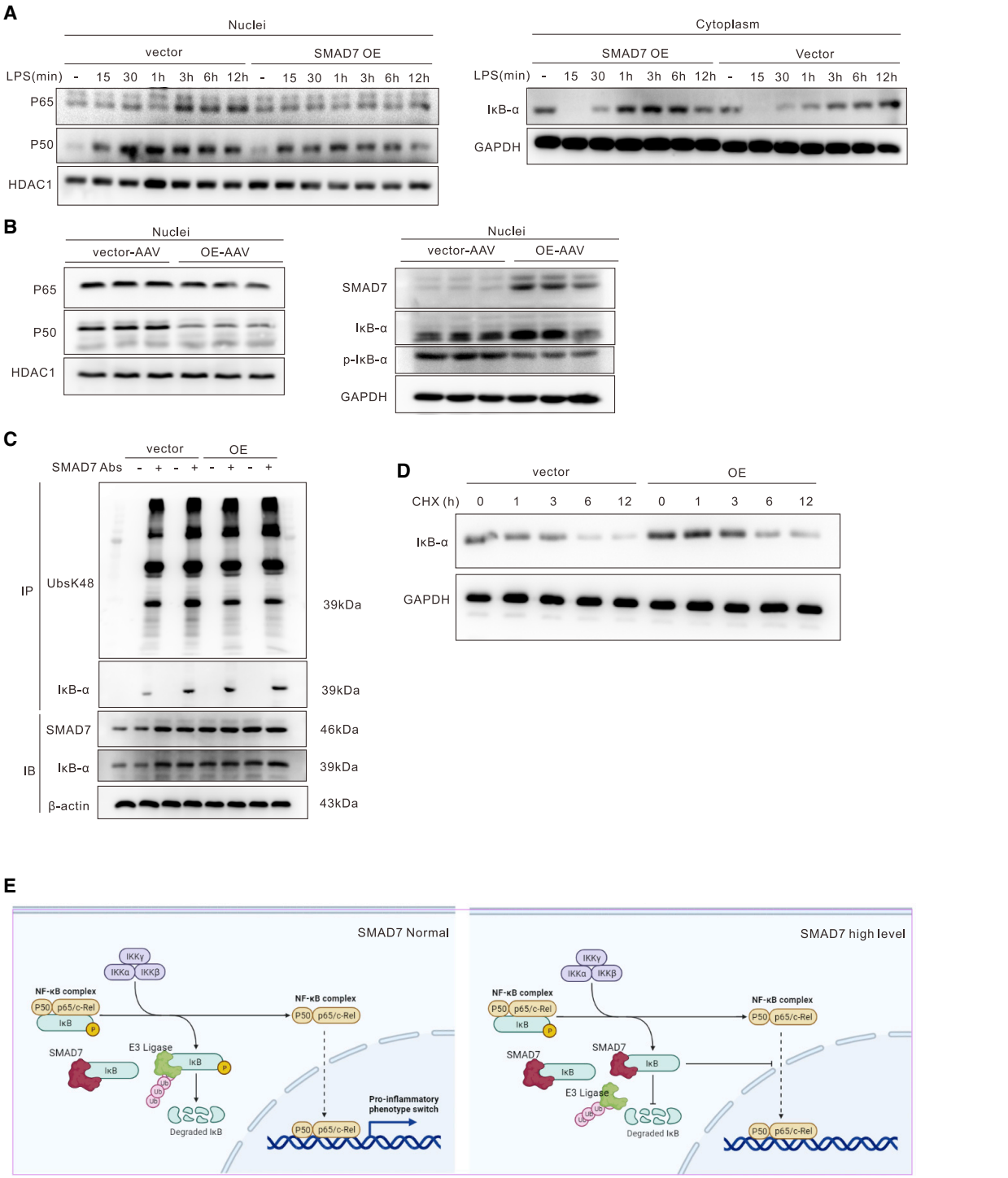

Figure 6. SMAD7 attenuated NF-κB cascade activation through competitive inhibiting K48 ubiquitination of negative regulator Iκbα

(A) Western blots show the protein level of P65 and P50 extracted from vector (NC) or SMAD7-overexpressed (SMAD7 OE) microglial nuclei which were treated with lipopolysaccharide (LPS) (100 ng/mL) for different time points (left). Western blots show the Iκbα protein level in the cytoplasm (right). (B) Protein expression of P65, P50 detected in nuclei of vector (adeno-associated virus [AAV]-vector) and SMAD7-overexpressed (AAV-OE) TBI mice brains (left). (C) Co-immunoprecipitation of SMAD7 and

(legend continued on next page)

DISCUSSION

Severe and unlimited neuroinflammation is considered an important promoter in secondary damage of TBI and an unfavorable factor for post-TBI recovery.[7] Pro-inflammatory cytokines directly cause neuronal cell death and enhance brain edema and lymphocyte infiltration, further leading to progression of inflammation and worse outcomes.[26] Therefore, characterizing the regulative process of neuroinflammation is useful to develop novel treatment methods to improve the prognosis of TBI. Astrocyte-microglial interaction participates in post-TBI neuroinflammation and neurovascular recovery.[27,28] Studies have shown that astrocytes communicate with microglia via exosomes containing non-coding RNA.[9,29] Our previous studies in TBI revealed that astrocyte-releasing exosomes containing miRNA attenuate TBI-associated microglial pro-inflammatory phenotypes.[9]

To systematically understand the exosome communications between astrocytes and microglia, multiple RNA-seq including miRNA, lncRNA, and mRNA sequencing were performed in the current study. We constructed the regulative network with respect to TBI conditions. Our results showed that up-regulated lncRNA 4933431K23Rik appeared in CCE-treated astrocytes and their released exosomes. This is an observation because little is known about the biological function of 4933431K23Rik. Thus, we explored this question further by generating exosomes containing overexpressed 4933431K23Rik. To our knowledge, our study showed that a higher content of 4933431K23Rik in exosomes attenuated the pro-inflammatory phenotype of microglia. Furthermore, introducing 4933431K23Rik-overexpressing exosomes *in vivo* promoted functional recovery after TBI. Most previous published studies have focused on the pro-neuroinflammation effect of microglial-induced lncRNA. Several studies demonstrated that lncRNAs, such as HOXA-AS2 or 4344, promoted microglial-induced neuroinflammation via sponge-specific miRNAs.[30,31] In contrast, our study demonstrated an anti-inflammatory effect of lncRNA, implying a context-dependent multifaceted action of lncRNA for the induction of microglial phenotype. Our study also identified that 4933431K23Rik sponging miR-10a-5p regulated microglial functions, and thus modulated downstream targeted E2F7 and TFAP2C.

TFAP2C is a member of the AP-2 transcription factor family, whereas E2F7 is an untypical transcription factor which belongs to the E2 family.[32,33] Both these transcriptions factors have been reported as capable of initiating "effector" mRNA transcription, which participates in cancer and development, etc.[33] Little is known about the function of TFAP2C and E2F7 in inflammation or about the effect on microglia; therefore, in this study, we further identified that downstream SMAD7 was the effector protein that mediated/transduced lncRNA/miRNA regulative effects. SMAD7 has been illustrated to negatively regulate inflammation via distinct pathway signaling. Using multiple *in vitro* and *in vivo* methods, we systematically unveiled the functions of SMAD7 on microglia which include anti-inflammation, activation, and phagocytosis. These effects will not only alleviate neuroinflammation and microglial infiltration but will also increase the clearance of TBI-induced debris and substantially improve post-TBI recovery. Previous studies demonstrated that SMAD7 inhibits the NF-κB pathway and eventually modulates chronic inflammation outcomes.[34] The present study revealed that SMAD7 protected the IκBα from K48 ubiquitination which in turn negatively regulated the p65 and p50 translocation into nuclei. Indeed, the specific physical interaction region between SMAD7 and IκBα requires further investigation, and results could lead to using this region as a therapeutic target.

Most previous studies centered on the pro-inflammation process post-TBI, whereas we focused on the astrocytes and illustrated that astrocytes exhibit the potential of negative feedback against neuroinflammation. Even though astrocytes are co-stimulated in TBI brains which contributes to neuroinflammation, our data illustrated that it remains as negative anti-inflammatory signaling, while this force is overwhelmed by other pro-inflammatory signaling. Therefore, our results showed an unexpected "opposite" pathway that may be a useful therapeutic target for TBI by amplifying/stimulating SMAD7 to relieve neuroinflammation and improve outcomes.

MATERIALS AND METHODS

Animals and ethical information

Animal ethics approval for the use of adult and newborn mice was received from the Experimental Animal Ethics Committee of Huazhong University of Science and Technology. Male C57BL/10ScNJ mice (age 8–10 weeks, weight 23.02 ± 1.64 g) were obtained from GemPharmatech (Nanjing, China). The mice were fed and housed in the Experimental Animal Center of Tongji Scientific Building of Tongji Hospital. All mice were maintained in a controlled environment at 22°C ± 3°C and 60% relative humidity under a 12 h light/dark cycle and were given free access to standard rodent nutrition and water. The experiments conformed to all relevant regulatory standards as follow. The experimental procedures were approved by the ethics committee of the Animal Experiment Center of Tongji Medical College, Huazhong University of Science and Technology. With regard to the patient-derived specimens, the present study was performed in accordance with the Declaration of Helsinki, and the study protocol and written informed consent were approved by the medical ethics committee of Tongji Hospital.

Cell culture

Primary microglia and astrocytes were extracted from the brains of neonatal male C57BL/10ScNJ mice (age 1–2 days) as previously described.[16,35] Briefly, neonatal mice were decapitated and

Iκbα in vector (NC) or SMAD7-overexpressed (SMAD7 OE) microglial cells using SMAD7 antibody. The immunoprecipitation complex was also determined for K48 ubiquitination (UbsK48). (D) Cycloheximide (CHX)-treated vector or SMAD7-overexpressed (OE) microglia was determined for Iκbα using western blot. (E) Schematic figures illustrate that overexpressed SMAD7 could competitively bind to IkBa, leading to negative regulation of p65/p50 nuclei translocation.

subsequently, the brain tissues of the neonatal mice were collected for primary microglia culture. The cerebrum was cut into 1 mm^3 pieces which were digested with 0.125% trypsin at room temperature for 4 min and then at 37°C in a 5% CO_2 incubator for 4 min. The digestion process was terminated by the addition of 2 times the volume of culture medium (DMEM [catalog #G4510; Wuhan Servicebio Technology, Wuhan, China] supplemented with 10% fetal bovine serum [FBS] [catalog #10091148; Thermo Fisher Scientific, Waltham, MA] and 1% penicillin-streptomycin [catalog #C100C5; Newcell & Molecular Biotech, Soochow, China]). The cerebrum extract was filtered using a 70 μm nylon mesh. This extract was then centrifugated at 59 × *g* for 5 min at 4°C (catalog #3K15; Millipore), and the cell pellet was collected and cultured in a T-75 flask of 15 mL culture medium; each T-75 flask contained extracts from four neonatal mouse brain tissues. Microglia and astrocytes were divided using a constant temperature culture oscillator (catalog #ZWY-103B; ZHICHENG, Shanghai, China) at 100 rpm for 40 min at 37.0°C after 10 days and were then cultured in 6- or 24-well plates at 37°C in a 5% CO_2 incubator for subsequent experiments. Human 293T cells were gift from Dr. Shutao Pan obtained from the American Type Culture Collection (ATCC; Manassas, Virginia). BV-2 murine microglial cells and HMC-3 human microglial cells were obtained from the ATCC. All cells were maintained in DMEM with supplements, 10% fetal calf serum (FCS; Thermo Fisher Scientific), 50 UL/mL penicillin, 50 μg/mL streptomycin, and 200 mM glutamine (all purchased from Newcell & Molecular Biotech).

CCE generation

The CCE was generated as previously described.[9,15] Briefly, the mouse cortex samples were placed into a glass grinder for grinding tissue, after which the samples were centrifugated at 350 × *g* for 5 min at 4°C to remove cells. Samples were filtered through a 0.22 μm filter unit (catalog #SLGP033RB; Millipore). Next, 1 mL of the supernatant was aliquoted in 1.5 mL EP tubes and kept at −80°C for further experiments. The protein concentration of CCE was determined using the BCA reaction system (catalog #G2026-200T; Wuhan Servicebio Technology) using a microplate reader (Infinite F50; Tecan Group, Männedorf, Switzerland) at a wavelength of 570 nm.

In silico analysis of single-cell RNA sequencing datasets

The processed single-cell RNA-seq (scRNA-seq) dataset of murine traumatic brain injury model was obtained from the Gene Expression Omnibus (GEO) database (https://www.ncbi.nlm.nih.gov/geo/) using accession number (GSE180862). Expression matrix were conducted using counts per million (CPM) normalization, and quality control included keeping high-quality cells after removing cells with fewer than 200 genes, more than 20,000 genes, and/or more than 20% mitochondrial genes. Principal-component analysis (PCA) was performed on the 2,000 genes with high variability, obtaining the first 50 principal components (PCs). The cells were divided into 15 clusters on the basis of the first 20 PCs and presented using uniform manifold approximation and projection (UMAP). Cells from clusters 3, 7, and 12 (expressing Iba-1) were isolated as microglia populations, regrouping into 5 groups, and exhibiting the distribution of inflammatory cytokines (Cd86, Il1b, Il10, Arg1, Mrc1, and Cd163) by UMAP.

Cell transfection

For lncRNA 4933431K23Rik, SMAD7 overexpression, lncRNA 4933431K23Rik and SMAD7 were cloned into pcDNA3.1-CMV promoter vector (Invitrogen, Carlsbad, CA). The expression plasmids were generated by AUGCT Biotechnology (Beijing, China). For expression plasmids transfection, cells were transfected with control pcDNA3.1-CMV promoter vector or corresponding expression vector together with Lipofectamine 3000 (Thermo Fisher Scientific). For lncRNA 4933431K23Rik knockdown, lncRNA 4933431K23Rik shRNA was generated on GV102 lentivirus vector (hU6-MCS-CMV-GFP-SV40-Neomycin), with targeting sequence (#1: GCAA GAAGGGCCTGACAATGT; #2: GGAAGCTGAAAGAAGGCAT TG; #3: GGTGTTTCTAAGACACCATAT). Regarding transfection, shRNA plasmids together with packaging plasmids (psPAX2 and pMD2.G, catalog #12260 and catalog #12259, gift from Dr. Shutao Pan, obtained from Addgene) were transfected into 293T cells (at 50% confluence) using Lipofectamine 3000 and P3000 reagent (Thermo Fisher Scientific) according to the manufacturer's instructions. After transfection, medium was changed at 6 and 24 h. Supernatant of the cells was collected and filtered using 0.22 μm filter at 72 h after transfection. Cells were infected with the supernatant for 3 days in the presence of 10 μg/mL Polybrene (catalog #40804ES76; Yeason, Shanghai, China). Puromycin (1 μg/mL; Yeason) was used for 7 days to select cells after infection. For E2F7, TFAP2C, and SMAD7 siRNA knockdown, siRNAs together with the negative control siRNA were produced and purchased from AUGCT Biotechnology. Cells were transfected with either 100 nM targeting siRNA or NC siRNA using Lipofectamine 3000. The sequences of the siRNAs are shown in Table S1. For miR-10a-5p mimics, negative control mimics, miR-10a-5p agomir, miR-10a-5p antagomir, and negative control agomir or antagomir transfection, RNA molecules were added to the cells together with transfection reagents (Lipofectamine 3000). The sequences of the mimics are shown in Table S2.

Exosome isolation and treatment

Primary astrocytes were used for the isolation of exosomes which were isolated and extracted using Exoquick Kit (System Biosciences, Palo Alto, CA). Briefly, the supernatant was centrifuged at 3,500 × *g* for 10 min at 4°C and at 12,000 × *g* for 10 min at 4°C. The supernatant was collected and corresponding reagents were added to the supernatant in turn according to the instructions of the kit manual. Samples were centrifuged again to separate the exosomes. The precipitates were collected and RNase-free phosphate-buffered saline (PBS) was added. Then, the exosomes were assessed using transmission electron microscopy (TEM) and nanoparticle tracking analysis (NTA). Particle size distribution of astrocyte-derived exosomes was measured using a nano-flow cytometer. The mean particle concentration of the astrocyte-derived exosomes in the conditioned medium was approximately 5 × 10^8 particles/mL and 750 particles/cell (see Figure S1 for details).

Controlled cortical impact model of TBI

TBI was established using the controlled cortical impact (CCI) modified method as previously described.[9,36] CCI was performed to produce medium contusion of the brain. Briefly, after administering anesthesia with 5% isoflurane in oxygen with a delivery rate of 0.5 L/min for induction and 2% isoflurane for maintenance, the mice were placed onto a stereotaxic apparatus platform. Sterile procedures were adhered to and the initial incision was along the midline. Subsequently, a 3 mm^2 craniotomy was performed at the following specific location: left hemisphere, 1 mm anterior-λ, 1 mm left-midline, and 1 mm post-bregma. In total, 3 mm^2 of the skull was removed while avoiding damage to the dura mater. The CCI (YHCI99; Wuhan Yihong Technology, Wuhan, China) parameters were as follows: (1) deformation depth, 1 mm; (2) impact speed, 3.5 m/s; and (3) duration, 400 ms. The sham mice underwent a craniotomy without CCI impact. The incisions were sutured, and the mice were placed on a 36°C–37°C heated pad. For exosome treatment, a total of 5×10^8 exosomes (harvested from vector or lncRNA 49rik-overexpression astrocytes) were applied via intraventricularly injection using a micro-syringe (Hamilton, Reno, NV). For agomir or antagomir treatment, 10 μmol of control agomir, control antagomir, miR-10a-5p agomir, or miR-10a-5p antagomir was intraventricularly injected into the mice 1 day after CCI model. For microglia SMAD7 overexpression *in vivo*, adeno-associated virus transfection *in vivo* was used. pAAV-Cx3crl promoter-SMAD7-3xFLAG-P2A-mCherry-tWPA and pAAV-Cx3crl promoter-MCS-mCherry-tWPA were generated by Obio Technology (Shanghai, China). AAV virus vector (NC: pAAV-cx3cr1 promoter MCS - mCherry - tWPA; titer: 2.87E +12 v.g./mL, 10 μL per brain; overexpression: pAAV-Cx3cr1 promoter SMAD7 - 3Xflag-P2A-mCherry - tWPA; titer: 8.43E + 12 v.g./mL, 3.4 μL per brain) were intraventricularly injected into the brain of C57 mice under the stereotactic instrument, using a flat-head micro-syringe and injected slowly for 15 min to form a 1 mm^3 virus transfer area. The sequence details of AAV was described in the supplemental information. For microglia depletion, 8 μL of clodronate liposome (Liposoma Technology, Groningen, the Netherlands) or control liposome (Liposoma Technology) was intraventricularly injected into mice 3 days prior to TBI model establishment.

RNA sequencing of exosomes and cells

Total RNA was extracted from the exosomes or cells using TRIzol reagent (catalog #15596018; Thermo Fisher Scientific) according to the manufacturer's protocol, and RNA levels and quality were detected using a NanoDrop (Thermo Fisher Scientific). The RNA library was constructed strictly according to the QIAseq RNA Library Kit. Approximately 100 ng of total RNA was used to prepare the RNA library supplemented with water to 20 μL, then reverse transcribed. Qubit Fluorimeter (Thermo Fisher Scientific) was then used to measure library concentration. Bioanalyzer 2100 (Agilent) was used to inspect the quality of the library. The library was sequenced using Illumina HiSeq 2500 (Illumina, San Diego, CA). Raw data (raw reads) in fastq format were first processed to obtain clean data (clean reads) by removing the adapter reads and low-quality reads from the raw data. Genes with adjusted p values <0.01 and fold change >2 found by DESeq were assigned as differentially expressed. Processed RNA-seq datasets were uploaded in the supplemental information, titled "processed RNA-seq datasets." Raw sequencing data were uploaded to Genome Sequence Archive (GSA [https://ngdc.cncb.ac.cn/gsa/]; accession number CRA009252).

Morris water maze

Spatial learning and memory were tested using the MWM starting on day 7 after surgery. The apparatus comprised of a swimming pool (diameter 1.5 m, height 60 cm) filled with water (temperature 21°C–25°C). Mice were trained to find a submerged platform (depth 1.5 cm) using the marker around the side wall. During the 6 day training period, the platform was placed in the third quadrant of the testing arena. At each time trial every day, all mice were allowed 60 s to find the platform and were given a 30 s stay on the platform. At the start of each trial the mice were randomly placed into one of the three quadrants (first, second, and fourth quadrants). The average latency, moving distance, and swimming speed before locating the platform at each time trial on the test day were recorded using WMT-100 Morris software (Chengdu Taimeng Technology, Chengdu, China). On day 7, space exploration assessment was performed, wherein the platform was removed, and the mice were given 60 s to locate the area where the platform had previously been; the duration of time spent in the target quadrant and the number of times that the mice crossed the previous platform location were recorded.

Modified neurological severity scores test

The mNSS test was performed according to previous protocol.[9] Neurological damage was evaluated using the mNSS system on days 1–28 after the induction of TBI by CCI. This system assesses abnormal movements and motor, sensory, and reflex deficits. The total possible score is 18 points; the higher the score, the more severe the neurological damage. The test was performed on days 1, 3, 7, 14, and 28 by three individuals in a triple-blind manner, and the scores were averaged.

Rotarod test

Mice coordination, strength, and balance were assessed from day 7 post-surgery. Mice were placed on a swivel bar fatigue tester with the rotation speed set at 30 rpm, and the activity was recorded for 5 min. Mice were trained twice daily for 6 days with 300 s as the cutoff value and then tested, as previously described.[37] The latency to fall was recorded.

Tissue preparation for immunofluorescence

All mice were then immediately injected with an overdose of ketamine (180 mg/kg) + xylazine (30 mg/kg) for euthanasia post-TBI. Death was verified by the lack of breathing, pulse, corneal reflex, and response to firm toe pinch. The mice were transcardially perfused with PBS and 4% paraformaldehyde (PFA). Brain tissues were then isolated and placed in 4% PFA for 1 day at room temperature. The tissues were fixed with 30% sucrose for 48 h at room temperature. Frozen brain sections (40 μm) were sliced using a sliding microtome

(Leica, Wetzlar, Germany); the freezing platform and freezing chamber were set at −35° and −20°C, respectively.

H&E staining

Mice brain tissue was fixed in 4% PFA solution for 24 h. Brain tissue was cut into a thickness of 0.5 cm along the coronal position of the contusion and laceration focus and washed with running water for 10 min. The following processes were completed. The dehydration process was performed by immersing the tissue in 75% ethanol overnight, 95% ethanol for 1 h, absolute ethanol for 1 h, and xylene for 40 min. The wax dipping process included the placement of liquid paraffin into a wax-dissolving box for 1 h after immersion. Embedding processes was competed by adding liquid paraffin, immersing the tissues, then placing them into a refrigerant for solidification for 1 h followed by storage at room temperature. The slicing process involved the following: the cutting thickness of the tissues was 30 μM, and tissues were then placed into a constant temperature drying oven for 24 h. The dewaxing process included initial dewaxing of the xylene for 5 min (i.e., maintained for 5 min), a second dewaxing for 5 min, and a third for 5 min. Hydration process involved soaking of the specimens in absolute ethanol for 5 min, 95% ethanol for 5 min, 80% ethanol for 5 min, 70% ethanol for 5 min, and tap water for 2 min 3 times. The dying process included hematoxylin staining for 5 min. Then, the specimens were slowly washed of the stain using running water, immersed in acid and alcohol once, washed again using running water for 5 min, followed by eosin staining for 2 min and washing of the nonspecific bound eosin fuel using running water. A second/final dehydration process included an immersion of the specimens in 70% ethanol for 10 s, 80% ethanol for 10 s, 90% ethanol for 10 s, anhydrous ethanol for 5 min, xylene I for 5 min, and xylene II for 5 min. Finally, the seal process was completed using neutral resin seal. An automatic scanning microscope (Olympus, Tokyo, Japan) was used for the analysis/viewing of tissues. The lesion volume was determined by unbiased stereology according to the Cavalieri principle by determining lesion area in every 12th 40-μm-thick brain slice and then multiplying this area by the factor 12 × 40 μm.

Immunofluorescence

The frozen brain sections or 4% PFA fixed cells were blocked in 5% BSA (catalog #G5001-100G; Wuhan Servicebio Technology) with 0.1% Triton X-100 in Tris-buffered saline (TBS) for 2 h at room temperature. Subsequently, tissues were incubated with the following primary antibodies diluted in 5% BSA in TBS overnight at 4°C: goat anti-ionized calcium binding adaptor molecule 1 (1:200; catalog #ab5076; Abcam, Cambridge, UK), rabbit anti-CD68 (1:100; catalog #ab125212; Abcam), rabbit anti-CD31 (1:200; catalog #ab28364; Abcam), mouse anti-CD31 (1:200; catalog #89C2; Cell Signaling Technology, Danvers, MA), mouse anti-neuronal nuclear protein (1:200; catalog #94403S; Cell Signaling Technology), rabbit anti-myelin basic protein (1:5,000; catalog #ab218011; Abcam), and rabbit anti-glial fibrillary acidic protein (GFAP; 1:100; catalog #A0237; ABclonal Biotech, Wuhan, China), rabbit anti-lysosomal associated membrane protein 1 (LAMP1; 1:100; catalog #AF4320; R&D Systems, Minneapolis, MN), or rabbit anti-SMAD7 (1:100; catalog #ab272928; Abcam). The sections were subsequently washed three times for 10 min each in TBS and then incubated for 2 h at room temperature with the following secondary antibodies: Cy3-conjugated donkey anti-goat (1:500; catalog #GB21404; Wuhan Servicebio Technology), Cy3-conjugated goat anti-rabbit (1:500; catalog #GB21303; Wuhan Servicebio Technology), FITC-conjugated donkey anti-rabbit (1:200; catalog #GB22403; Wuhan Servicebio Technology), FITC-conjugated donkey anti-goat (1:200; catalog #GB22404; Wuhan Servicebio Technology), or FITC-conjugated donkey anti-mouse (1:200; catalog #GB22301; Wuhan Servicebio Technology) diluted in 5% BSA and DAPI (50%; catalog #G1012; Wuhan Servicebio Technology) in TBS. The sections were washed four times (10 min/wash) with TBS before being sealed with fluorescent antifade solution (catalog #G1401; Wuhan Servicebio Technology) and a cover glass. Images were captured using a fluorescence microscope (Olympus). Besides, confocal microscope (LSM780; Carl Zeiss, Oberkochen, Germany) was used to acquire cellular imaging. ImageJ version 1.8.0 (National Institutes of Health, Bethesda, MD) software was used for data analysis.

ELISA

After 24 h stimulation, the supernatant of each group was centrifuged at 350 × *g* for 5 min at 4°C to remove cells and then filtered through a 0.22 μm filter (catalog #SLGP033RB; Millipore). The inflammation-associated proteins IL-1β, IL-6, and TNF-α were detected in the cellular supernatants of different groups using IL-1β (catalog #70-EK201B/3-96); IL-6 (catalog #70-EK206/3-96), and TNF-α (catalog #70-EK282/4-96) ELISA kits (Multisciences [Lianke] Biotech, Hangzhou, China) according to the manufacturer's protocols. The absorbance values of the samples were detected using a microplate reader at 450 nm, and the final concentrations of these inflammatory cytokines were calculated according to the absorbance.

qRT-PCR

Total RNA was extracted from the cortex or cells using TRIzol reagent according to the manufacturer's protocol, and RNA levels and quality were detected using a NanoDrop. mRNA was reverse transcribed into cDNA using Hifair III 1st Strand cDNA Synthesis SuperMix (catalog #11141ES10; Shanghai Yeasen Biotechnology, Shanghai, China). Reverse transcription was performed in a 20 μL system under the following thermocycling conditions: 25°C for 5 min, 55°C for 15 min, and 85°C for 5 min. qPCR was performed using Hieff qPCR SYBR Green Master Mix (catalog #11202ES03; Shanghai Yeasen Biotechnology) and Quant Studio-1 Design & Analysis Software (catalog #A40426; Thermo Fisher Scientific) under the following thermocycling conditions: one cycle at 95°C for 5 min, followed by 40 cycles at 95°C for 10 s and 60°C for 30 s, and a final melt curve stage at 60°C for 1 min and 95°C for 1 s. The specific primers used for qPCR are listed in Table S3. Relative target gene expression to the geometric mean of the reference gene glyceraldehyde 3-phosphate dehydrogenase (GAPDH) was determined using the formula $2 - \Delta\Delta Cq$, where $\Delta Cq = Cq$ (target gene) − Cq (GAPDH) and $\Delta\Delta Cq = \Delta Cq$ (target gene) − ΔCq (control). Changes in gene expression are presented as fold changes compared with gene expression in the control group.

Heatmaps were generated using the Pheatmaps package in R version 4.1.1 (https://www.r-project.org).

Western blotting

RIPA buffer (catalog #G2002; Wuhan Servicebio Technology) lysis buffer (RIPA:PMSF:phosphoproteins inhibitor A:B = 100:1:1:1; all from Wuhan Servicebio Technology) was used to extract total proteins from primary microglial cells, mouse brain tissues, and patient biopsy tissues. Protein concentration was determined using the BCA reaction system (catalog #G2026-200T; Wuhan Servicebio Technology) using a microplate reader (Infinite F50) at a wavelength of 570 nm. The final protein concentration was 5 μg/μL. Equal amounts (30 μg/lane) of protein lysates were separated using SDS-PAGE on 10% gels and transferred onto Immobilon-P PVDF membranes (catalog #IPVH00010; Millipore). After blocking with 5% BSA for 2 h at room temperature, membranes were incubated with the following primary antibodies overnight at 4°C: rabbit anti-SMAD7 (1:1,000; catalog #A278; ABclonal Biotech), rabbit anti-E2F7 (1:1,000; catalog #A15211; ABclonal Biotech), rabbit anti-TFAP2C (1:500; catalog #A7739; ABclonal Biotech), rabbit anti-CD63 (1:1,000; catalog #ab125212; Abcam), rabbit anti-CD81 (1:1,000; catalog #ab109201; Abcam), rabbit anti-CD9 (1:500; catalog #ab223052; Abcam), rabbit anti-claudin-5 (1:1,000; catalog #34-1600; Thermo Fisher Scientific), rabbit anti-occludin (1:1,000; catalog #33-1500; Thermo Fisher Scientific), rabbit anti-NF-κB (1:1,000; catalog #AP0123; ABclonal Biotech), rabbit anti-NF-κB p50 (1:1,000; Cat# A19653; ABclonal Biotech), rabbit anti-NF-κB p65 (1:1,000; catalog #A19653; ABclonal Biotech), rabbit anti-Ubs K48 (1:1,000; catalog #A3606; ABclonal Biotech), rabbit anti-IκB-α (1:200; catalog #4812S; Cell Signaling Technology), rabbit anti-p-IκB-α (1:200; catalog #2859P; Cell Signaling Technology), rabbit anti-GAPDH (1:1,000; catalog #A19056; ABclonal Biotech), rabbit anti-β-actin (1:1,000; catalog #AC026; ABclonal Biotech), and rabbit anti-HDAC1 (1:1,000; catalog #A19571; ABclonal Biotech). Subsequently, the membranes were incubated with the following corresponding secondary antibodies at room temperature for 2 h: HRP-conjugated goat anti-rabbit IgG (1:5,000; catalog #GB23303; Wuhan Servicebio Technology) and HRP-conjugated goat anti-mouse IgG (1:5,000; catalog #AS003; ABclonal Biotech). The protein bands were visualized using BeyoECL reagent (catalog #P0018S; Beyotime Institute of Biotechnology, Shanghai, China) and a GeneGnome XRQ Chemiluminescence Imaging System (GeneGnome XRQ; Syngene, Cambridge, UK) exposure instrument. Gray intensity of the bands was calculated using ImageJ version 1.8.0. Finally, the expression levels of the proteins were standardized using densitometric analysis to β-actin or glyceraldehyde 3-phosphate dehydrogenase levels.

Agarose spot assay

Cellular chemotaxis activity was examined using an agarose spot test by modifying the protocol of the chemotactic invasion assay described previously.[38] Briefly, low-melting point agarose (Shanghai Yeasen Biotechnology) was diluted in 0.5% PBS. Subsequently, LPS (100 ng/mL; catalog #SMB00610; Millipore) or SMAD7 siRNA and SMAD7 siRNA-NC were mixed with 0.5% agarose solution to final concentrations of 100 ng/mL and 2 μg/mL, respectively. The mixed agarose solution for each spot (10 μL) was then pipetted into 20 mm glass-bottomed dishes (Thermo Fisher Scientific) to generate four spots, two containing SMAD7 siRNA-NC as the negative controls and two containing SMAD7 siRNA + LPS. These were cooled for 15 min at 4°C. Subsequently, primary cultured microglial cells (3×10^5/mL) were plated into the dishes and incubated at 37°C for 3 h. Images were captured using the Ocular 2.0 software (Thermo Fisher Scientific) with a light microscope (catalog #CKX53; Olympus). The number of microglial cells that appeared under the agarose spots were counted using the microscope.

Transwell assay

The Transwell assay was used to analyze cell migration. Briefly, the upper and lower chambers were separated using a polycarbonate filter (pore size 8 μm; Corning). Culture medium (DMEM) without fetal bovine serum supplemented with SMAD7-NC (2 μg/mL) + vehicle, SMAD7-NC (2 μg/mL) + LPS (100 ng/mL), SMAD7 siRNA (2 μg/mL) + vehicle, and SMAD7 siRNA (2 μg/mL) + LPS (100 ng/mL) was added into the upper chamber, and culture medium with 10% FBS was added into the lower chamber. Subsequently, primary cultured microglia (5×10^4/mL) were seeded into the upper chamber and both chambers were incubated at 37°C for 24 h. Subsequently, the upper side of the membrane was fixed with 4% paraformaldehyde for 30 min at room temperature, then wiped with a cotton bud. Cells that migrated to the lower chamber were stained with a crystal violet solution (catalog #G1014; Wuhan Servicebio Technology) for 30 min at room temperature. Finally, the rate of microglial migration was calculated by counting cells in four random fields in each well under a bright-field microscope at 20× magnification.

Phagocytosis assay

The phagocytosis assay was performed according to previous method.[16] Microglia were seeded on coverslips in a 24-well plate for 6 h to adhere. Next, YF fluorescent beads (Polysciences, Warrington, PA) or fluorescence (PKH26; catalog #D0030; Solarbio, Beijing, China) labeled myelin debris (collected during CCE generation) were added for 30 min. Subsequently, cells were rinsed 3 times with PBS buffer for 10 min. After fixation with 4% PFA for 1 h at room temperature, cells were blocked with 5% donkey serum in PBS for 1 h at room temperature, and subsequently incubated with primary antibody (Iba-1; Abcam) overnight in 4°C. Cells on coverslips were then washed 3 times with PBS, and incubated with FITC-conjugated donkey anti-goat (1:200, Cat# GB22404, Wuhan Servicebio Technology) secondary antibody and DAPI at room temperature for 2 h. Coverslips were mounted with Aquapolymount (Polysciences) and the images were taken by fluorescence microscope (Olympus). Phagocytosis index was analyzed as total number of beads/DAPI-positive cells × 100.

Dual-luciferase assay

Transfection of viral lncRNA 49rik plasmid into HEK 293T cells was completed as follows. The cells were seeded in 24-well plate. After the density of 293T cells reached approximately 80%, vectors including

pmir-GLO-lncRNA-4933431K23Rik-WT (wild-type) vector, pmir-GLO-lncRNA-4933431K23Rik-Mut vector, pmir-GLO-E2F7-3′ UTR WT vector, pmir-GLO-E2F7-3′ UTR Mut vector, pmir-GLO-TFAP2C-3′ UTR WT vector and pmir-GLO-TFAP2C-3′ UTR Mut vector (constructed by AUGCT Biotechnology) were simultaneously co-transfected with miRNA-10a-5p mimics or negative control mimics in the presence of Lipofectamine 3000. The cells were then incubated at 37°C for 48 h. Luciferase activity was then assessed using the dual-luciferase reporter assay system (Promega, Madison, WI) according to the manufacturer's instructions. The absorbance values of the samples were detected using a microplate reader at 560 nm and the final intensity of the signals were calculated according to the absorbance. Firefly luciferase activity was normalized to Renilla activity.

Evans blue

Evans blue (1%; catalog #E2129; Sigma-Aldrich, St. Louis, MO) was injected (5 mL/kg) via tail vein 1 h prior to sacrifice. After transcardially perfused with PBS, mice brains were collected and weighed. PBS buffer was added to the samples, and subsequently, the samples were homogenized in a glass tube followed by centrifugation at 12,000 rpm for 5 min at 4°C. The supernatant was collected and same amount of 50% trichloroacetic acid was added for overnight incubation at 4°C. The sample solution was examined by a spectrometer at 610 nm. Quantification was achieved by using a standard curve which was normalized to tissue weight (micrograms per gram).

Magnetic-activated cell sorting

MACS were performed according to manufacture instructions (CD11b beads: catalog #130-093-634; adult brain dissociation kit: catalog #130-107-677; Miltenyi, Bergisch Gladbach, Germany) and previous protocol.[17,39] Briefly, TBI mice were transcardially perfused with 1× phosphate-buffered saline under deep anesthesia, and brains were removed. The brain tissue from the injury focus and the perilesion area were collected and placed into a tube grinder (C-tube) for grinding. After adding enzyme mix (catalog #130-107-677; Miltenyi), the C-tube was placed onto the sleeve of the gentleMACS Octo Dissociator with Heaters. After finishing the program, samples were resuspended and filtered using a MACS SmartStrainer (70 μm). The cell suspension was then centrifuged at 300 × *g* for 10 min at 4°C followed by supernatant aspiration. Cell pellet was washed, and Debris Removal Solution (catalog #130-107-677; Miltenyi) was added and centrifuged at 4°C and 3,000 × g for 10 min with full acceleration and full brake. Then the top two layer was aspirated completely. The cell pellet was then resuspended with cold PBS and centrifuged at 4°C and 1,000 × *g* for 10 min with full acceleration and full brake. The supernatant was discarded and the cells were resuspended with MACS buffer (PBS supplemented with 0.5% BSA and 2 mM EDTA). Next, the cell suspension was incubated with CD11b microbeads (catalog #130-093-634; Miltenyi) for 15 min at 4°C. MACS column (Miltenyi) was washed with MACS buffer 3 times, and cells were then loaded into the column. The column was then detached from the magnetic device and flushed with MACS buffer to collect CD11b-positive cells. CD11b-positive cells were then processed with qPCR or ELISA.

Statistical analysis

All statistical analyses were performed using Graph Pad Prism 6 (GraphPad Software, La Jolla, CA). Data are presented as mean ± SD, and all experiments were repeated at least three times. Statistical differences were determined using either an unpaired two-tailed Student's t test, one-way analysis of variance (ANOVA) followed by Tukey's post hoc test, or two-way ANOVA with Sidak's or Tukey's post hoc test. The Kruskal-Wallis was used to analyze non-parametric data. p values < 0.05 were considered to indicate statistical significance.

DATA AVAILABILITY

The datasets used and/or analyzed in the present study are available from the corresponding author upon reasonable request.

SUPPLEMENTAL INFORMATION

Supplemental information can be found online at https://doi.org/10.1016/j.ymthe.2023.01.031.

ACKNOWLEDGMENTS

This work is supported by the Natural Science Foundation of Hubei Province (WJ2019Z008) and the Natural Science Foundation of Tongji Hospital (2020JZKT651).

AUTHOR CONTRIBUTIONS

H.Z. designed and supervised the project. Y.H. and X.H. wrote the paper, performed *in vivo* and *in vitro* research, and were responsible for data analysis and revision of the manuscript. X. Zhang, Yanchao Liu, X.M., X.L., and Yuan Liu were responsible for tissue processing. Y.R., H.L., and C.G. performed parts of experiments. X.W., X. Zou, B.X., K.S., and T.L. provided critical suggestions. All authors approved the final version of the paper.

DECLARATION OF INTERESTS

The authors declare no competing interests.

REFERENCES

1. Shao, F., Wang, X., Wu, H., Wu, Q., and Zhang, J. (2022). Microglia and neuroinflammation: crucial pathological mechanisms in traumatic brain injury-induced neurodegeneration. Front. Aging Neurosci. *14*, 825086.

2. Bolte, A.C., and Lukens, J.R. (2021). Neuroimmune cleanup crews in brain injury. Trends Immunol. *42*, 480–494.

3. Wolf, S.A., Boddeke, H.W.G.M., and Kettenmann, H. (2017). Microglia in physiology and disease. Annu. Rev. Physiol. *79*, 619–643.

4. Escartin, C., Galea, E., Lakatos, A., O'Callaghan, J.P., Petzold, G.C., Serrano-Pozo, A., Steinhäuser, C., Volterra, A., Carmignoto, G., Agarwal, A., et al. (2021). Reactive astrocyte nomenclature, definitions, and future directions. Nat. Neurosci. *24*, 312–325.

5. Hanisch, U.K., and Kettenmann, H. (2007). Microglia: active sensor and versatile effector cells in the normal and pathologic brain. Nat. Neurosci. *10*, 1387–1394.

6. Kettenmann, H., Hanisch, U.K., Noda, M., and Verkhratsky, A. (2011). Physiology of microglia. Physiol. Rev. *91*, 461–553.

7. Donat, C.K., Scott, G., Gentleman, S.M., and Sastre, M. (2017). Microglial activation in traumatic brain injury. Front. Aging Neurosci. *9*, 208.

8. Chen, M., Lai, X., Wang, X., Ying, J., Zhang, L., Zhou, B., Liu, X., Zhang, J., Wei, G., and Hua, F. (2021). Long non-coding RNAs and circular RNAs: insights into microglia and astrocyte mediated neurological diseases. Front. Mol. Neurosci. *14*, 745066.
9. Long, X., Yao, X., Jiang, Q., Yang, Y., He, X., Tian, W., Zhao, K., and Zhang, H. (2020). Astrocyte-derived exosomes enriched with miR-873a-5p inhibit neuroinflammation via microglia phenotype modulation after traumatic brain injury. J. Neuroinflammation *17*, 89.
10. Yang, Y., Yang, H., Yang, Y., and Ma, Y. (2022). Exosomal microRNAs have great potential in the neurorestorative therapy for traumatic brain injury. Exp. Neurol. *352*, 114026.
11. Marques, T.M., and Gama-Carvalho, M. (2022). Network approaches to study endogenous RNA competition and its impact on tissue-specific microRNA functions. Biomolecules *12*, 332.
12. Hu, Y., He, J., He, L., Xu, B., and Wang, Q. (2021). Expression and function of Smad7 in autoimmune and inflammatory diseases. J. Mol. Med. *99*, 1209–1220.
13. Stolfi, C., Troncone, E., Marafini, I., and Monteleone, G. (2020). Role of tgf-beta and smad7 in gut inflammation, fibrosis and cancer. Biomolecules *11*, 15–17.
14. Lin, N., Ji, Z., and Huang, C. (2017). Smad7 alleviates glomerular mesangial cell proliferation via the ROS-NF-κB pathway. Exp. Cell Res. *361*, 210–216.
15. He, X., Huang, Y., Liu, Y., Zhang, X., Yue, P., Ma, X., Miao, Z., Long, X., Yang, Y., Wan, X., et al. (2022). BAY61-3606 attenuates neuroinflammation and neurofunctional damage by inhibiting microglial Mincle/Syk signaling response after traumatic brain injury. Int. J. Mol. Med. *49*, 5.
16. Huang, Y., Zhang, Q., Lubas, M., Yuan, Y., Yalcin, F., Efe, I.E., Xia, P., Motta, E., Buonfiglioli, A., Lehnardt, S., et al. (2020). Synergistic toll-like receptor 3/9 signaling affects properties and impairs glioma-promoting activity of microglia. J. Neurosci. *40*, 6428–6443.
17. Huang, Y., Motta, E., Nanvuma, C., Kuhrt, L.D., Yuan, Y., Xia, P., Lubas, M., Zhu, S., Schnauss, M., Qazi, N., et al. (2022). Microglia/macrophage-derived human CCL18 promotes glioma progression via CCR8-ACP5 axis analyzed in humanized slice model. Cell Rep. *39*, 110670.
18. Hanafy, K.A. (2013). The role of microglia and the TLR4 pathway in neuronal apoptosis and vasospasm after subarachnoid hemorrhage. J. Neuroinflammation *10*, 83.
19. Ka, S.M., Yeh, Y.C., Huang, X.R., Chao, T.K., Hung, Y.J., Yu, C.P., Lin, T.J., Wu, C.C., Lan, H.Y., and Chen, A. (2012). Kidney-targeting Smad7 gene transfer inhibits renal TGF-β/MAD homologue (SMAD) and nuclear factor κb (NF-κB) signalling pathways, and improves diabetic nephropathy in mice. Diabetologia *55*, 509–519.
20. Tang, B., Zhu, B., Liang, Y., Bi, L., Hu, Z., Chen, B., Zhang, K., and Zhu, J. (2011). Asiaticoside suppresses collagen expression and TGF-β/Smad signaling through inducing Smad7 and inhibiting TGF-βRI and TGF-βRII in keloid fibroblasts. Arch. Dermatol. Res. *303*, 563–572.
21. Le-Niculescu, H., Roseberry, K., Gill, S.S., Levey, D.F., Phalen, P.L., Mullen, J., Williams, A., Bhairo, S., Voegtline, T., Davis, H., et al. (2021). Precision medicine for mood disorders: objective assessment, risk prediction, pharmacogenomics, and repurposed drugs. Mol. Psychiatry *26*, 2776–2804.
22. Ju-Lin, X., Shao-Hai, Q., Tian-Zeng, L., Bin, H., Jing-Ming, T., Ying-Bin, X., Xu-Sheng, L., Bin, S., Hui-Zhen, L., and Yong, H. (2009). Effect of asiaticoside on hypertrophic scar in the rabbit ear model. J. Cutan. Pathol. *36*, 234–239.
23. Dresselhaus, E.C., and Meffert, M.K. (2019). Cellular specificity of NF-κB function in the nervous system. Front. Immunol. *10*, 1043.
24. Lawrence, T. (2011). Macrophages and NF-κB in cancer. Curr. Top. Microbiol. Immunol. *349*, 171–184.
25. Magnani, M., Crinelli, R., Bianchi, M., and Antonelli, A. (2000). The ubiquitin-dependent proteolytic system and other potential targets for the modulation of nuclear factor-kB (NF-kB). Curr. Drug Targets *1*, 387–399.
26. Zheng, R.Z., Lee, K.Y., Qi, Z.X., Wang, Z., Xu, Z.Y., Wu, X.H., and Mao, Y. (2022). Neuroinflammation following traumatic brain injury: take it seriously or not. Front. Immunol. *13*, 855701.
27. Yang, L., Zhou, Y., Jia, H., Qi, Y., Tu, S., and Shao, A. (2020). Affective immunology: the crosstalk between microglia and astrocytes plays key role? Front. Immunol. *11*, 1818.
28. Gaudet, A.D., and Fonken, L.K. (2018). Glial cells shape pathology and repair after spinal cord injury. Neurotherapeutics *15*, 554–577.
29. Li, Z., Song, Y., He, T., Wen, R., Li, Y., Chen, T., Huang, S., Wang, Y., Tang, Y., Shen, F., et al. (2021). M2 microglial small extracellular vesicles reduce glial scar formation via the miR-124/STAT3 pathway after ischemic stroke in mice. Theranostics *11*, 1232–1248.
30. Yang, X., Zhang, Y., Chen, Y., He, X., Qian, Y., Xu, S., Gao, C., Mo, C., Chen, S., and Xiao, Q. (2021). LncRNA HOXA-AS2 regulates microglial polarization via recruitment of PRC2 and epigenetic modification of PGC-1α expression. J. Neuroinflammation *18*, 197.
31. Feng, X., Zhan, F., Luo, D., Hu, J., Wei, G., Hua, F., and Xu, G. (2021). LncRNA 4344 promotes NLRP3-related neuroinflammation and cognitive impairment by targeting miR-138-5p. Brain Behav. Immun. *98*, 283–298.
32. Franke, C.M., Gu, V.W., Grimm, B.G., Cassady, V.C., White, J.R., Weigel, R.J., and Kulak, M.V. (2020). TFAP2C regulates carbonic anhydrase XII in human breast cancer. Oncogene *39*, 1290–1301.
33. Weijts, B.G.M.W., Bakker, W.J., Cornelissen, P.W.A., Liang, K.H., Schaftenaar, F.H., Westendorp, B., De Wolf, C.A.C.M.T., Paciejewska, M., Scheele, C.L.G.J., Kent, L., et al. (2012). E2F7 and E2F8 promote angiogenesis through transcriptional activation of VEGFA in cooperation with HIF1. EMBO J. *31*, 3871–3884.
34. Halder, L.D., Jo, E.A.H., Hasan, M.Z., Ferreira-Gomes, M., Krüger, T., Westermann, M., Palme, D.I., Rambach, G., Beyersdorf, N., Speth, C., et al. (2020). Immune modulation by complement receptor 3-dependent human monocyte TGF-β1-transporting vesicles. Nat. Commun. *11*, 2331.
35. Minelli, A., Lyons, S., Nolte, C., Verkhratsky, A., and Kettenmann, H. (2000). Ammonium triggers calcium elevation in cultured mouse microglial cells by initiating Ca2+ release from thapsigargin-sensitive intracellular stores. Pflugers Arch. *439*, 370–377.
36. Krämer, T.J., Hack, N., Brühl, T.J., Menzel, L., Hummel, R., Griemert, E.V., Klein, M., Thal, S.C., Bopp, T., and Schäfer, M.K.E. (2019). Depletion of regulatory T cells increases T cell brain infiltration, reactive astrogliosis, and interferon-γgene expression in acute experimental traumatic brain injury. J. Neuroinflammation *16*, 163.
37. Huang, Y., Li, Q., Tian, H., Yao, X., Bakina, O., Zhang, H., Lei, T., and Hu, F. (2020). MEK inhibitor trametinib attenuates neuroinflammation and cognitive deficits following traumatic brain injury in mice. Am. J. Transl. Res. *12*, 6351–6365.
38. Buonfiglioli, A., Efe, I.E., Guneykaya, D., Ivanov, A., Huang, Y., Orlowski, E., Krüger, C., Deisz, R.A., Markovic, D., Flüh, C., et al. (2019). let-7 MicroRNAs regulate microglial function and suppress glioma growth through toll-like receptor 7. Cell Rep. *29*, 3460–3471.e7.
39. Guneykaya, D., Ivanov, A., Hernandez, D.P., Haage, V., Wojtas, B., Meyer, N., Maricos, M., Jordan, P., Buonfiglioli, A., Gielniewski, B., et al. (2018). Transcriptional and translational differences of microglia from male and female brains. Cell Rep. *24*, 2773–2783.e6.